Analysis of NN Scattering in Nuclear Lattice Effective Field Thoery

Bing-Nan Lu[1]

Collaborate with: (Nuclear Lattice EFT Collaboration)

Evgeny Epelbaum; Hermann Krebs; Timo A. Lähde; Dean Lee; Ning Li; Thomas Luu; Ulf-G. Meißner; Gautam Rupak...

[1]Institute for Advanced Simulation, Institut für Kernphysik,
and Jülich Center for Hadron Physics, Forschungszentrum Jülich @Jülich,
Nordrhein-Westfalen, Germany

CRC110 Workshop, Ruhr-Universität Bochum, April 5-7, 2017

Outline

1. Introduction
2. Rotational symmetry on the lattice
3. Improving the lattice dispersion relation
4. Analysis of phase shift in the NLEFT

nucleons on the lattice

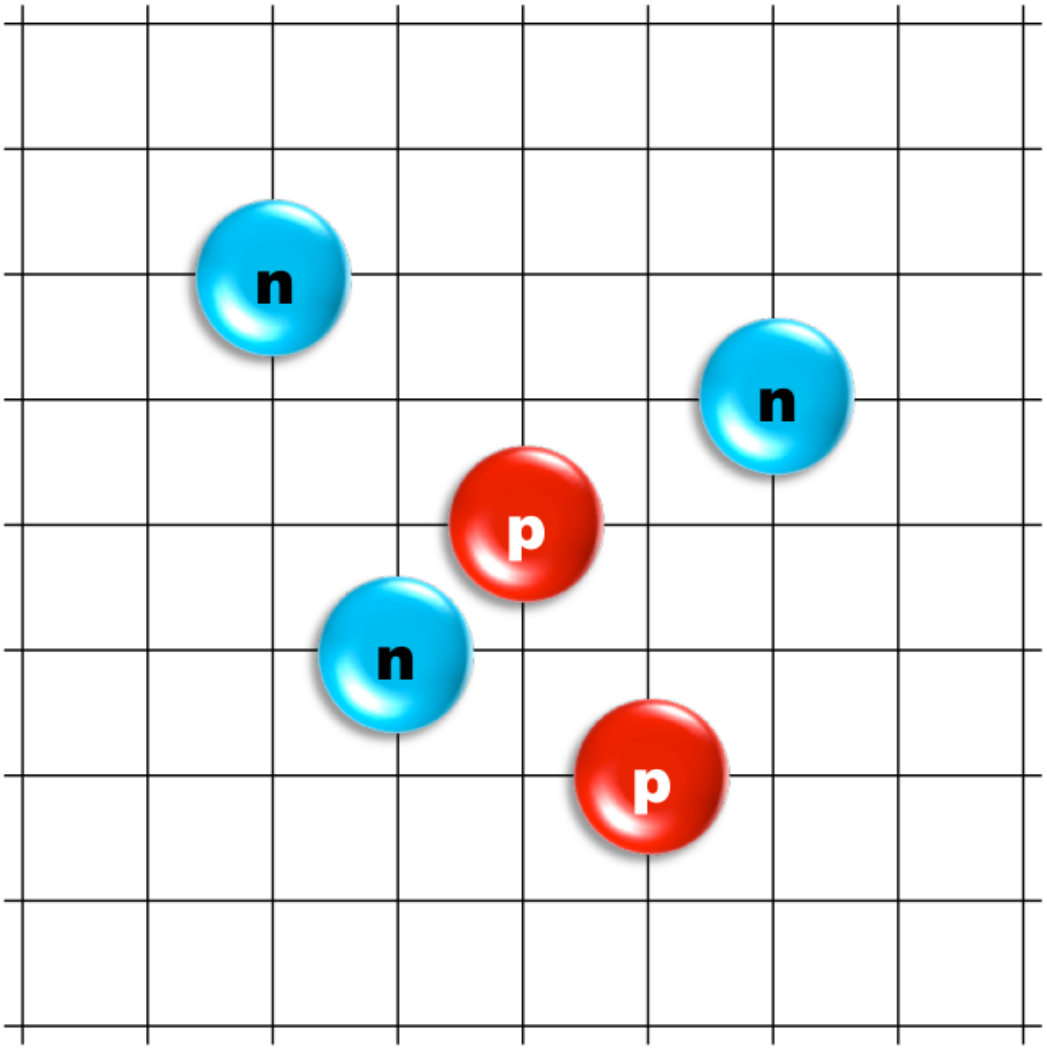

$a \sim 1 - 5$ fm

Order-by-order expansion of the NN force

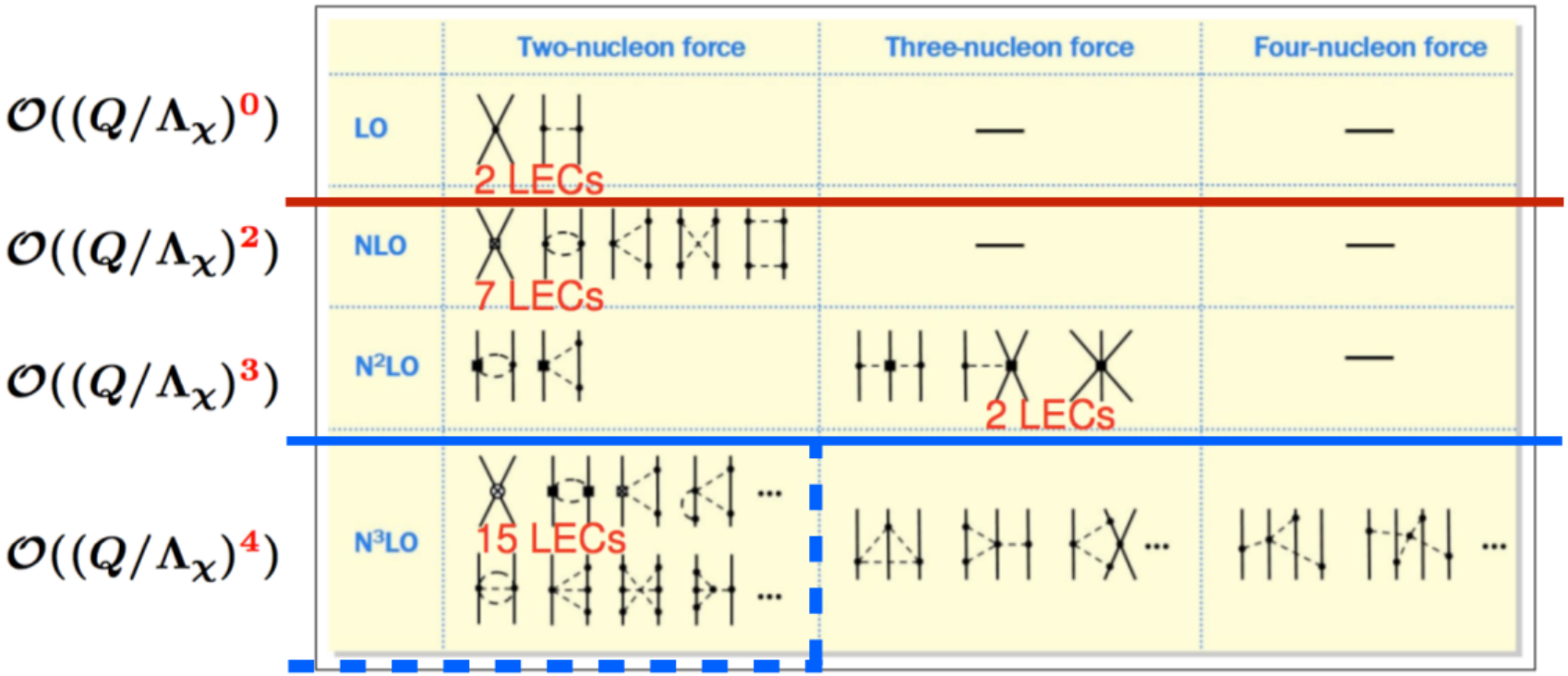

Implemented: LO -> non-perturbative; NLO -> perturbative

Euclidean time projection

From an arbitrary initial state, the ground state can be obtained by evolving along the imaginary time,

$$\exp(-Ht)|\psi_{\text{init}}\rangle \to \exp(-E_{\text{g.s.}}t)|\psi_{\text{g.s.}}\rangle, \qquad t \to \infty. \tag{1}$$

For Fermion system $|\psi_{\text{init}}\rangle$ is chosen to be a Slater determinant.
Define the projection amplitude

$$\mathscr{Z}(t) = \langle\psi_{\text{init}}|\exp(-Ht)|\psi_{\text{init}}\rangle \tag{2}$$

Thus the ground state energy reads (α_t=temporal lattice spacing)

$$E_{\text{g.s.}} = \lim_{t\to\infty} \frac{1}{\alpha_t} \ln \frac{\mathscr{Z}(t-\alpha_t)}{\mathscr{Z}(t)}. \tag{3}$$

One use the transfer matrix : $\exp(-H\alpha_t)$: instead of the Hamiltonian.

Rotational symmetry on the lattice

Splittings of the angular momentum multiplets

The discrete Hamiltonian is only invariant under the cubic group O. Any $2J+1$ multiplet of energy levels is split into subgroups belonging to different irreducible representations of the cubic group.

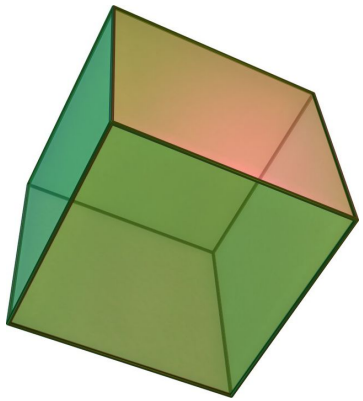

$D(O)$	g	D^0	D^1	D^2	D^3	D^4
A_1	1	1	0	0	0	1
A_2	1	0	0	0	1	0
E	2	0	0	1	0	1
T_1	3	0	1	0	1	1
T_2	3	0	0	1	1	1

Wave functions with cubic symmetry

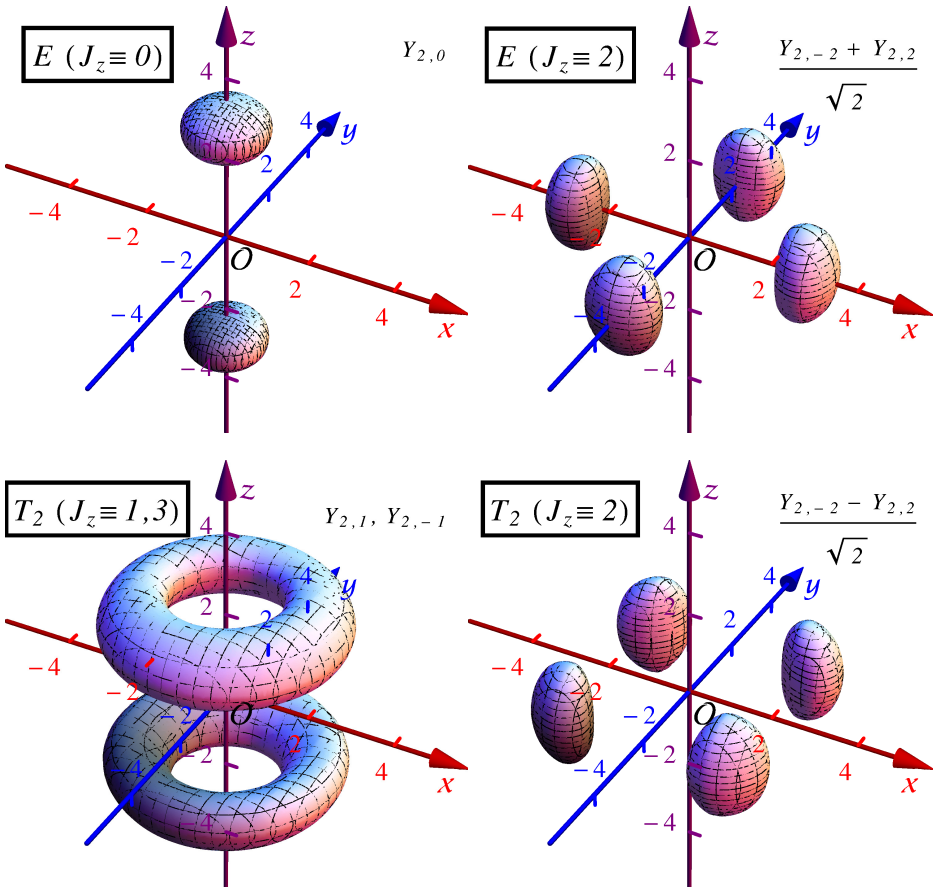

The $2J+1$ wave functions in a J multiplet are recombined to span the invariant sub spaces of the O group.
The states belonging to the same *irrep.* are distinguished by J_z,

$$R_z(\frac{\pi}{2})\psi = e^{i\frac{\pi}{2}J_z}\psi,$$

where $R_z(\frac{\pi}{2})$ is a rotation around z-axis by $\pi/2$. The $J=2$ decomposition is

$$\mathscr{H}_{J=2} = E\left[\sqrt{\frac{1}{2}}Y_{2,2} + \sqrt{\frac{1}{2}}Y_{2,-2}, Y_{2,0}\right] \oplus T_2\left[\sqrt{\frac{1}{2}}Y_{2,2} - \sqrt{\frac{1}{2}}Y_{2,-2}, Y_{2,\pm 1}\right]$$

BNL, Laehde, Lee, Meissner, PRD 90, 034507 (2014)

Lattice spacing artifacts

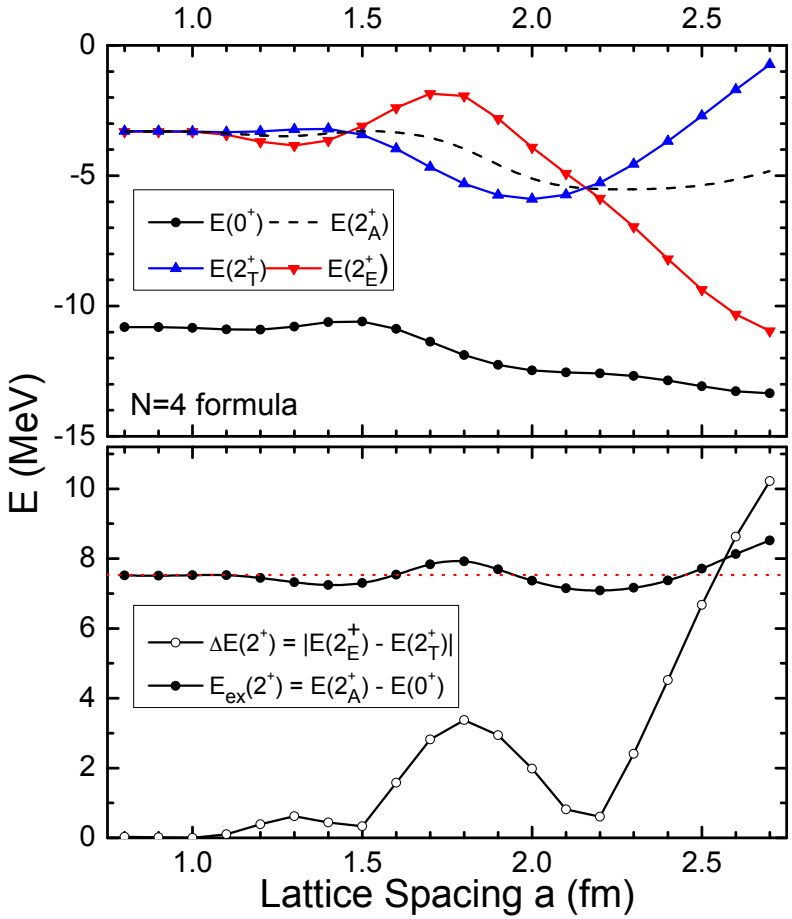

- Althouth $\Delta E(2^+)$ becomes as large as several MeV, the error of the multiplet-averaged excitation gap $E_{\text{ex}}(2^+)$ does not exceed 0.5 MeV for $a \leq 2.5$ fm.
- Multiplet averaging corresponds with angle averaging over all possible orientations of the lattice grid.
- It is quite reasonable that the cancellation between the ground state and averaged excited state energies will occur for general *ab initio* calculations.

Isotropic average for tensor operators

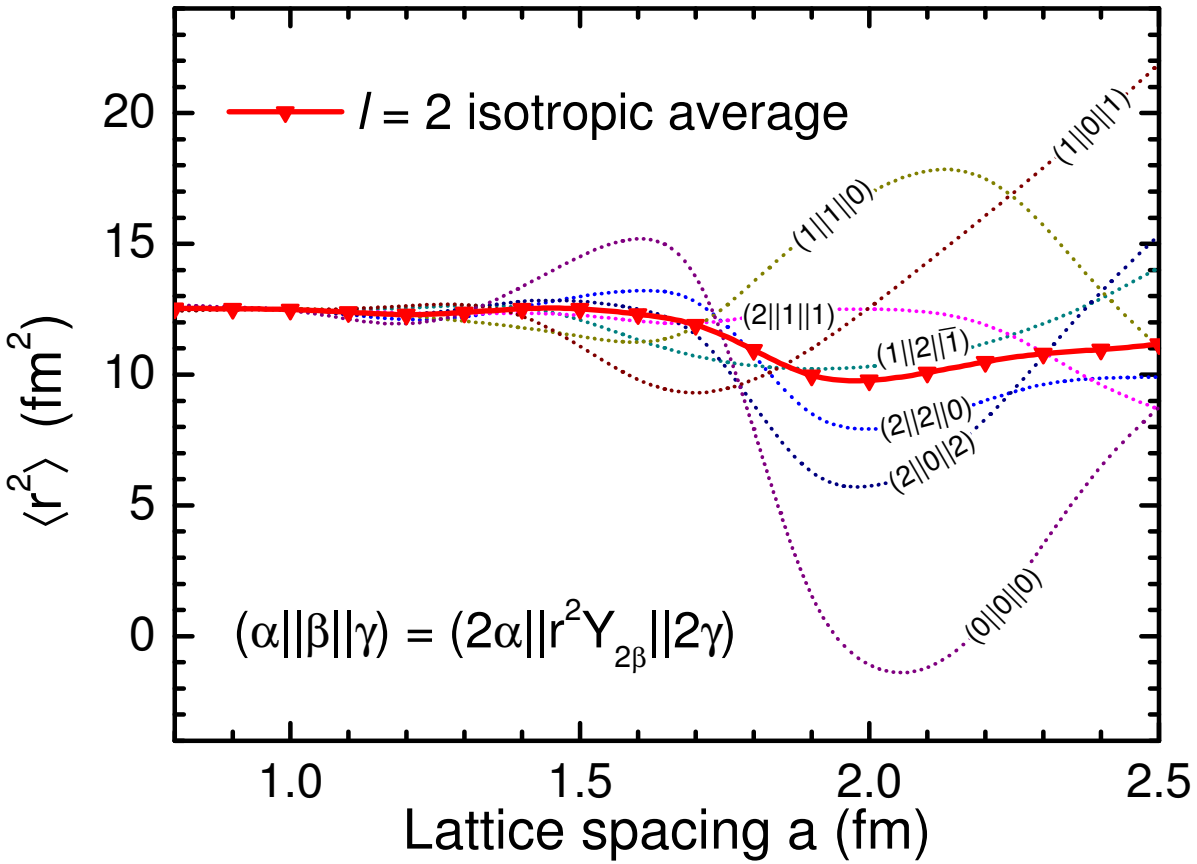

BNL, Lahde, Lee, Meissner, *Phys. Rev. D* 92, 014506 (2015)

Lüscher's formula

Imposing periodic boundary conditions with a period L, one can infer the s-wave infinite volume phase shifts from the energy spectrum with

$$p \cot \delta_0(p) = \frac{1}{\pi L} S(\eta), \qquad \eta = \left(\frac{Lp}{2\pi}\right)^2, \tag{4}$$

where $S(\eta)$ is the three-dimensional zeta function,

$$S(\eta) = \lim_{\Lambda \to \infty} \left[\sum_{\boldsymbol{n}} \frac{\theta(\Lambda^2 - \boldsymbol{n}^2)}{\boldsymbol{n}^2 - \eta} - 4\pi\Lambda \right].$$

Lüscher, Comm. Math. Phys. 105, 153 (1986)

The phase shifts are uniquely determined by the resulting spectrum.

Signal-to-noise problem in determining the phase shifts

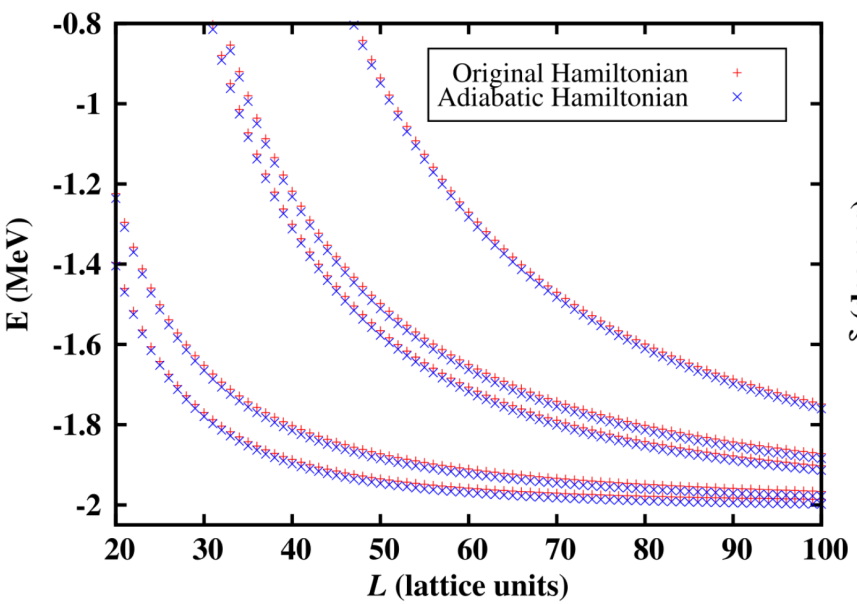

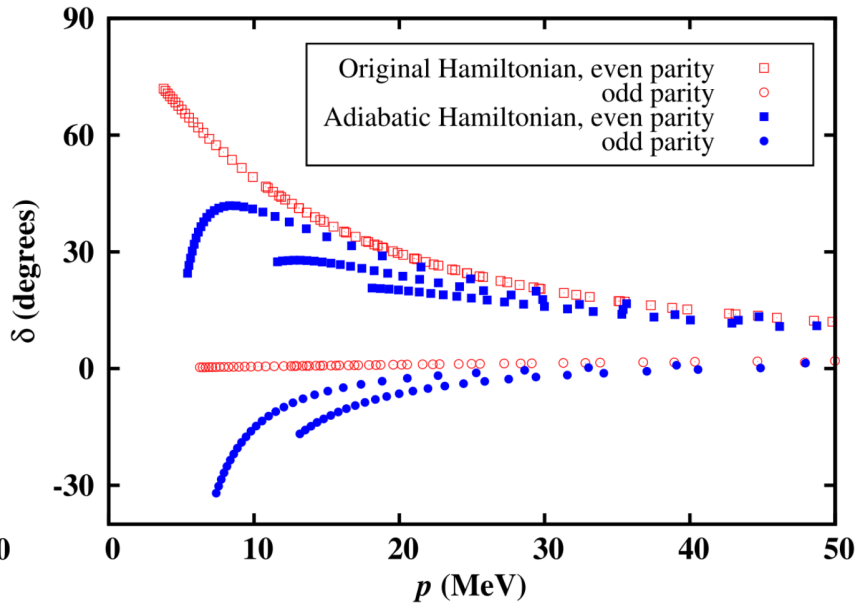

Left panel: Finite volume energies from Original and Adiabatic Hamiltonian;

Right panel: Phase shifts inferred from Lüscher's formula.

Precise determination of phase shifts calls for informations besides the energy spectrum.

Rokash, Pine, Elhatisari, Lee, Epelbaum, Krebs, arXiv:1505.02967v1 (2015)

Spherical wall method

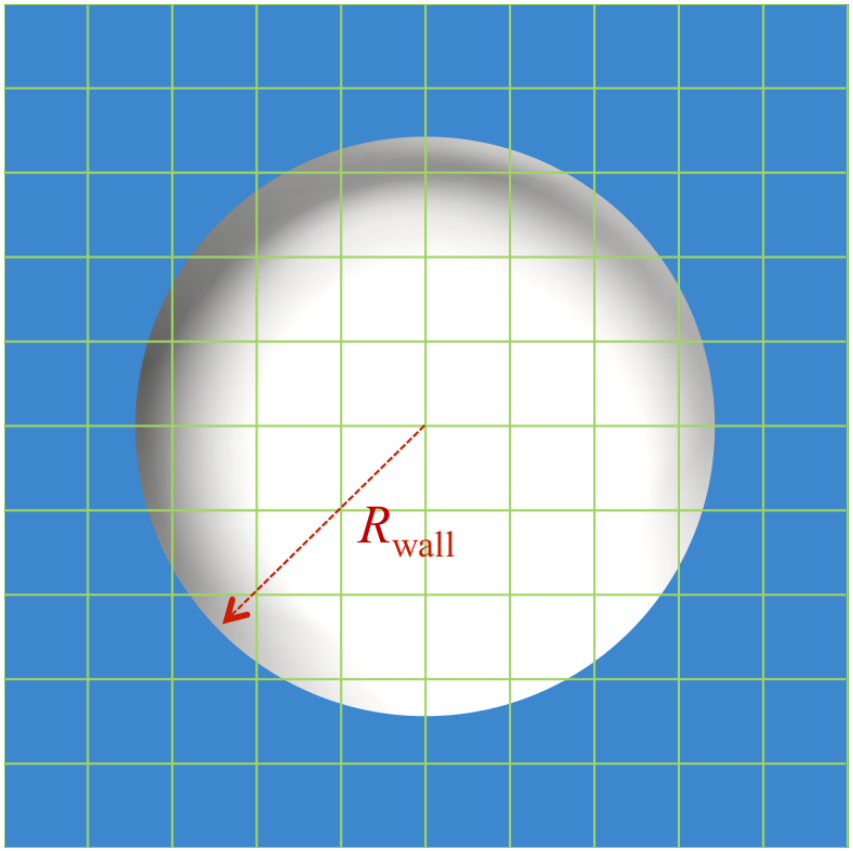

Imposing a hard wall,

$$V \to V + \Lambda\theta(r - R_{\text{wall}}),$$

wave functions vanish at R_{wall}.
In asymptotic region,

$$\psi(r) \propto \cos\delta_J j_J(kr) - \sin\delta_J y_J(kr),$$

thus

$$\tan\delta_J = \frac{j_J(kR_{\text{wall}})}{y_J(kR_{\text{wall}})}$$

Borasoy, Epelbaum, Krebs, Lee, Meißner EPJA34-185 (2007)

Radial Hamiltonian

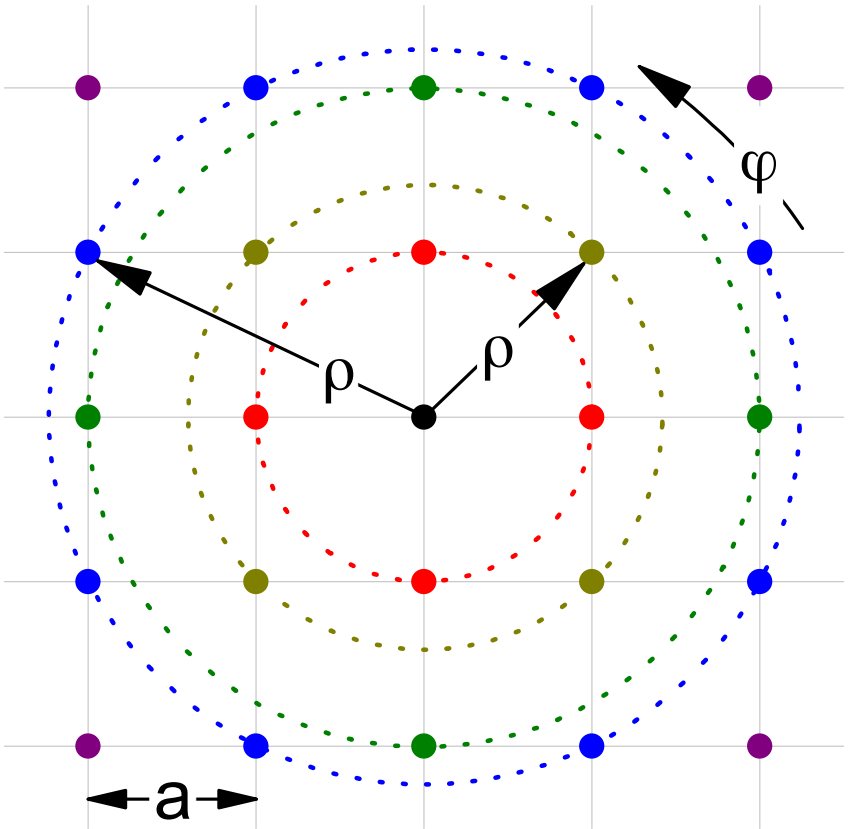

We extract the radial Hamiltonian by angular momentum projection.

Given the angular momenta L and L_z, we can define a radial Hamiltonian $H^{L}_{L_z}$ on the radial lattice to make the calculations more efficient.

This technique was applied to study the α-α elastic scattering.

Elhatisari, Lee, Rupak, Epelbaum, Krebs, Lähde, Luu, Meißner, Nature **528** (2015) 111

Radial Hamiltonian

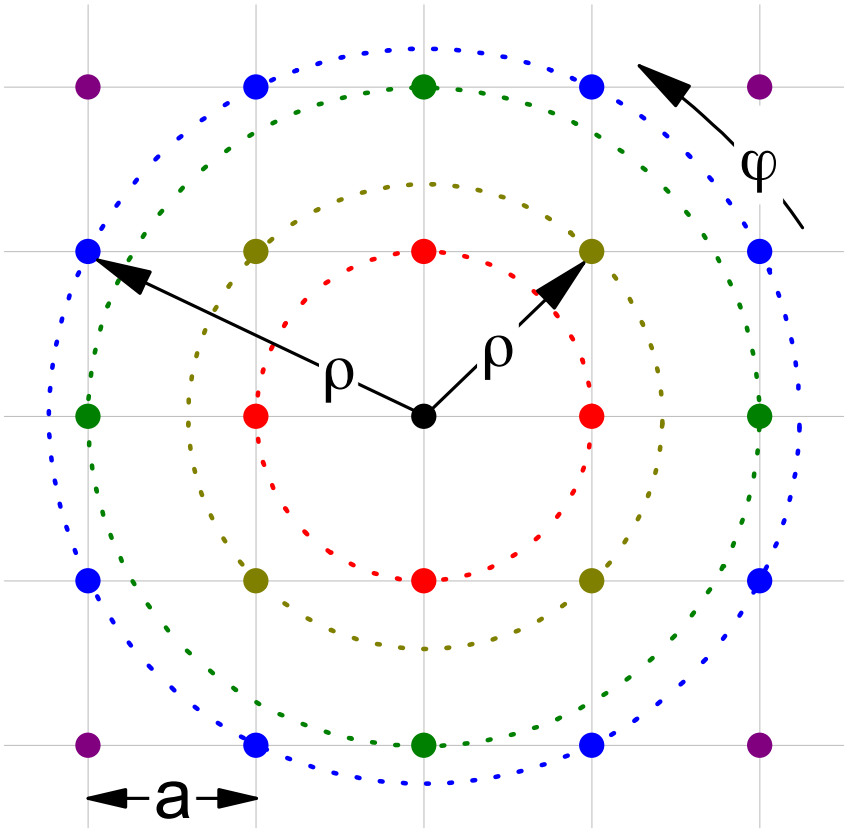

Expand wave functions on states with definite ρ, L and L_z,

$$|\rho\rangle_{L,L_z} = \sum_{\boldsymbol{r}} Y_{L,L_z}(\hat{\boldsymbol{r}})\delta_{\rho,|\boldsymbol{r}|}|\boldsymbol{r}\rangle$$

H in this basis read,

$${}_{L,L_z}\langle\rho|H|\rho'\rangle_{L',L'_z} \approx \delta_{L,L'}\delta_{L_z,L'_z}\langle\rho|H^L_{L_z}|\rho'\rangle$$

Radial Hamiltonians $H^L_{L_z}$ s' are defined as diagonal blocks of H.

The unphysical mixing induced by lattice artifacts is negligible.

Benchmark system

We use a two-body Hamiltonian for spin-1/2 particles,

$$H = -\frac{\nabla^2}{2\mu} + V(\boldsymbol{r}, \boldsymbol{\sigma}_1, \boldsymbol{\sigma}_2),$$

where V is a short range interaction containing a strong tensor part,

$$V = C\left\{1 + \frac{r^2}{R_0^2}\left[3(\hat{\boldsymbol{r}}\cdot\boldsymbol{\sigma}_1)(\hat{\boldsymbol{r}}\cdot\boldsymbol{\sigma}_2) - \boldsymbol{\sigma}_1\cdot\boldsymbol{\sigma}_2\right]\right\}\exp\left(-\frac{r^2}{2R_0^2}\right).$$

Borasoy, Epelbaum, Krebs, Lee, Meißner EPJA34-185 (2007)

- *The eigenstates of H are characterized by total intrinsic spin S and total angular momentum J.*
- *The tensor interaction induces appreciable mixing between S-D, P-F, D-G... partial waves.*

Benchmark system: Radial equations

Tensor force vanishes for $S = 0$ spin singlet states.

For $S = 1$, the radial eigen equation reads (with $L = J \pm 1$ a diagonal matrix),

$$\left[-\frac{1}{2m} \frac{1}{r} \frac{\partial^2}{\partial r^2} r + \frac{L(L+1)}{2mr^2} + V_J(r) \right] R_J(r) = E R_J(r),$$

For uncoupled channels,

$$V_J(r) = C \left(1 + \frac{2r^2}{R_0^2} \right) \exp\left(-\frac{r^2}{2R_0^2} \right)$$

for coupled channels

$$V_J(r) = C \left[1 + \frac{r^2}{R_0^2} \begin{pmatrix} -\frac{2(J-1)}{2J+1} & \frac{6\sqrt{J(J+1)}}{2J+1} \\ \frac{6\sqrt{J(J+1)}}{2J+1} & -\frac{2(J+2)}{2J+1} \end{pmatrix} \right] \exp\left(-\frac{r^2}{2R_0^2} \right)$$

Matrix elements of Radial Hamiltonian

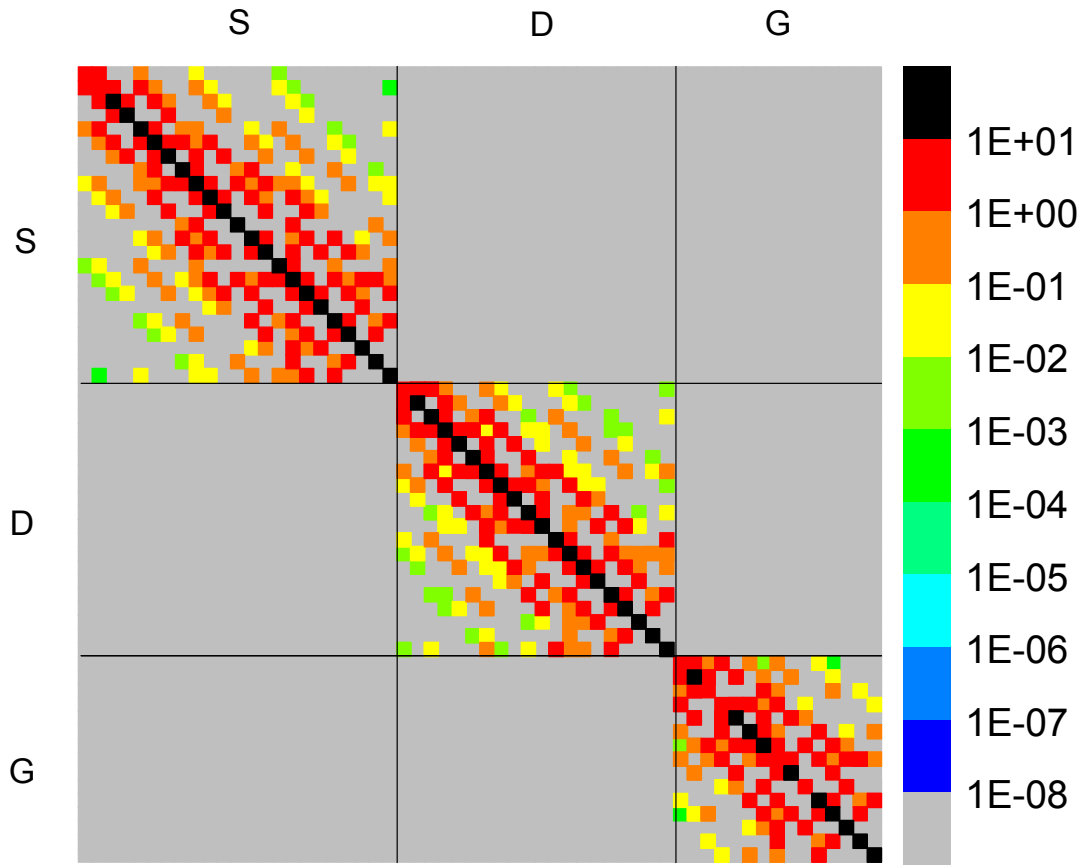

BNL, Lahde, Lee, Meissner, *Phys. Lett. B* 760, 309 (2016)

Energy eigenvalue of radial Hamiltonian

Even parity				
state	g	H	H_L^{J,J_z}	Δ
$1^3S(D)_1$	T_1	0.037	0.038	0.001
1^3D_2	E	2.764	2.766	0.002
$1^3D(G)_3$	T_1	3.347	3.351	0.004
1^3G_4	A_1	6.562	6.567	0.005
1^3G_4	T_1	6.624	6.637	0.013
Odd parity				
state	g	H	H_L^{J,J_z}	Δ
1^3P_1	T_1	0.917	0.918	0.001
$1^3P(F)_2$	E	1.795	1.796	0.001
1^3P_0	A_1	3.048	3.053	0.005
1^3F_3	A_2	4.616	4.620	0.004
$1^3F(H)_4$	A_1	4.998	5.003	0.005

The angular momentum decomposition can also be applied with explicit spin degrees of freedom.

Define the projection basis,

$$|\rho\rangle_L^{J,J_z} = \sum_{\boldsymbol{r},L_z,S_z} C^{J,J_z}_{L,L_z,S,S_z} Y_{L,L_z}(\hat{\boldsymbol{r}})\delta_{\rho,|\boldsymbol{r}|} \times |\boldsymbol{r}\rangle \otimes |S_z\rangle$$

$\longleftarrow$A comparison between full Hamiltonian H and radial Hamiltonian H_L^{J,J_z} in coupled/uncoupled $S=1$ channels. Energy eigenvalues are calculated with lattice spacing $a = 100$ MeV^{-1} and wall radius $R_{\text{wall}} = 10.02a$.

Eigenfunctions of radial Hamiltonian

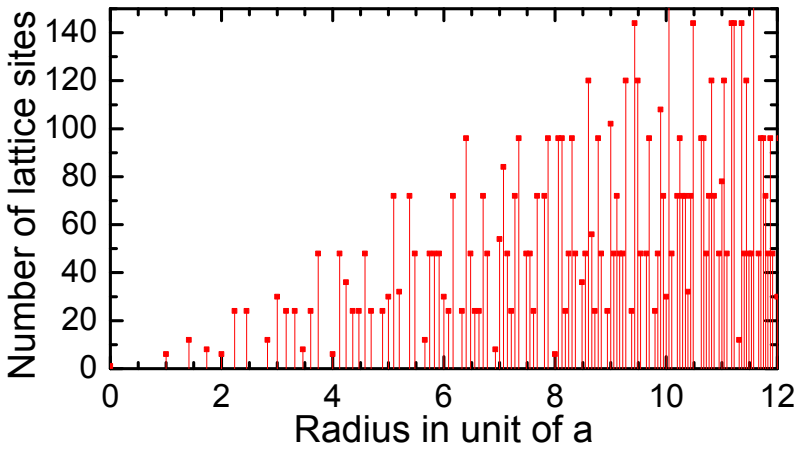

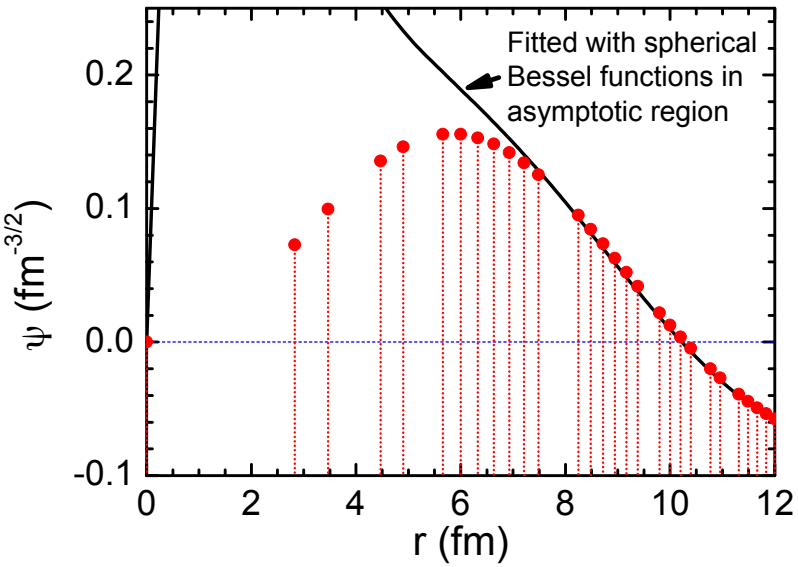

Density of radial mesh points scales as $\rho(r) \propto r$. In asymptotic region the wave function is almost a continuous function of r.

Fitting wave functions by spherical Hankel functions

In asymptotic region $R_{\text{Inner}} \leq r \leq R_{\text{Outer}}$ there is no interaction or only long range Coulomb interactions. We can fit the radial wave functions with spherical Hankel functions / Coulomb functions.

Minimize the error function

$$\chi^2 = \sum_{k \in \text{Asy.}} \left| \psi_k - A h^+_{J,k} + B h^-_{J,k} \right|^2 \tag{5}$$

with respect to complex constants A, B, A^* and B^*, we have

$$\begin{aligned} A &= \left[(h^+_J, \psi) \left| h^-_J \right|^2 - (h^-_J, \psi)(h^+_J, h^-_J) \right] / \langle h^+_J, h^-_J \rangle, \\ B &= \left[(h^+_J, \psi)(h^-_J, h^+_J) - (h^-_J, \psi) \left| h^{+2}_J \right| \right] / \langle h^+_J, h^-_J \rangle, \end{aligned}$$

with $(x, y) = \sum_{k \in \text{Asy.}} x^*_k y_k$ and $\langle h^+_J, h^-_J \rangle = \left| h^+_J \right|^2 \left| h^-_J \right|^2 - \left| (h^+_J, h^-_J) \right|^2$.

Extract phase shifts

In asymptotic region we have ($h^+$and h^- are spherical Hankel functions)

$$\psi_k \approx A h^+_{J,k} - B h^-_{J,k}, \tag{6}$$

with time reversal symmetry ψ_k are real and

$$A = -B^*, \qquad B = SA, \tag{7}$$

$S = e^{2i\delta_J}$ is the scattering matrix.

We can only obtain phase shifts at certain energies. Especially, very large R_{Wall} is needed to study low-energy phase shifts.

Auxiliary potentials

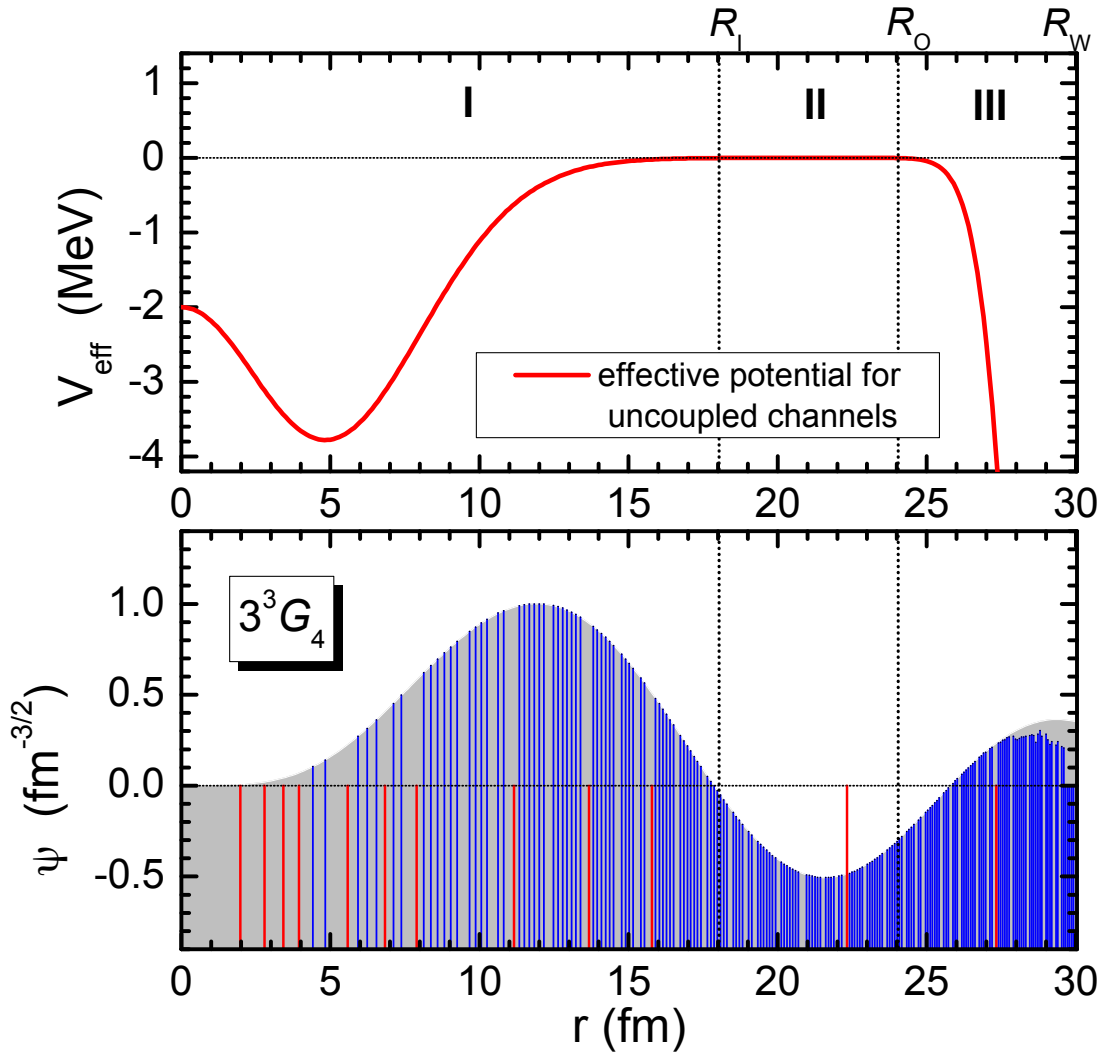

Shift energies with Auxiliary potentials

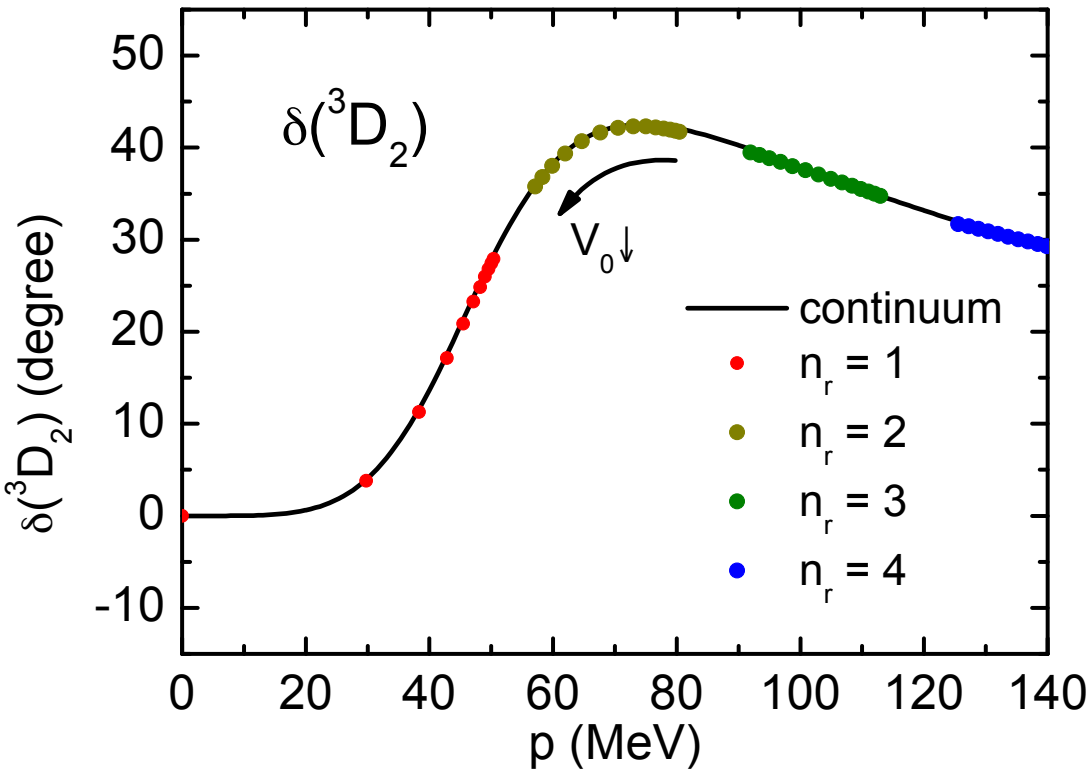

Energy eigenvalues are shifted continuously as functions of V_0. Phase shifts at low momentum can be obtained with moderate R_{Wall}.

Coupled $S = 1$ channels

For coupled channels the effective potentials become 2×2 matrices,

$$V_J(r) = C\left[1+\frac{r^2}{R_0^2}\begin{pmatrix} -\frac{2(J-1)}{2J+1} & \frac{6\sqrt{J(J+1)}}{2J+1} \\ \frac{6\sqrt{J(J+1)}}{2J+1} & -\frac{2(J+2)}{2J+1}\end{pmatrix}\right]\exp\left(-\frac{r^2}{2R_0^2}\right),$$

we have a group of energy eigenvalues with $n_r = 0, 1, 2...$
The two-component wave functions are real due to $\mathscr{T}$ symmetry.

For any energy eigenvalue we have only one single real wave function. However, in order to determine the phase shift and mixing angle, we need two linearly independent solutions.

Coupled $S = 1$ channels: phase shifts and mixing angles

In asymptotic region the wave function becomes

$$\begin{pmatrix} \psi_{J-1}(r) \\ \psi_{J+1}(r) \end{pmatrix} \longrightarrow \begin{pmatrix} A_{J-1}h^{+}_{J-1}(kr) - B_{J-1}h^{-}_{J-1}(kr) \\ A_{J+1}h^{+}_{J+1}(kr) - B_{J+1}h^{-}_{J+1}(kr) \end{pmatrix},$$

the coefficients satisfy

$$\begin{pmatrix} B_{J-1} \\ B_{J+1} \end{pmatrix} = \begin{pmatrix} S_{J-1,J-1} & S_{J-1,J+1} \\ S_{J+1,J-1} & S_{J+1,J+1} \end{pmatrix} \begin{pmatrix} A_{J-1} \\ A_{J+1} \end{pmatrix},$$

where the unitary matrix S is symmetric and can be parametrized with phase shifts $\delta_{J\pm1}$ and mixing angle ε_J as

$$S = \begin{pmatrix} e^{i\delta_{J-1}} & \\ & e^{i\delta_{J+1}} \end{pmatrix} \begin{pmatrix} \cos 2\varepsilon_J & i\sin 2\varepsilon_J \\ i\sin 2\varepsilon_J & \cos 2\varepsilon_J \end{pmatrix} \begin{pmatrix} e^{i\delta_{J-1}} & \\ & e^{i\delta_{J+1}} \end{pmatrix}.$$

We need at least two independent wave functions with the same energy to pin down S.

Coupled $S = 1$ channels: Broken degeneracy

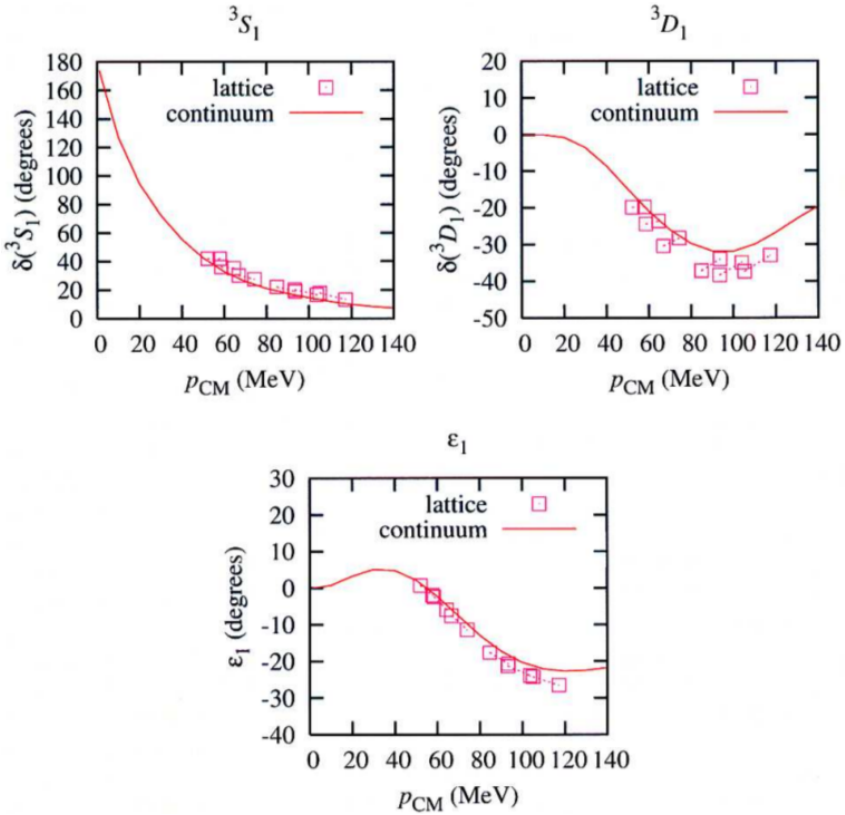

Borasoy, Epelbaum, Krebs, Lee, Meißner EPJA34-185 (2007)

We can always find pairs of energy eigenvalues that are close to each other. If we presume that they are exactly degenerate, phase shifts and mixing angles can be inferred. However, this induces significant uncertainties in the final results.

The hard wall boundary condition breaks the double degeneracy. Can we restore it without going to the infinite volume limit?

Complex auxiliary potential

We solve the problem by introducing a complex auxiliary potential as

$$V_J(r) \longrightarrow V_J(r) + \begin{pmatrix} & iU_{\text{aux}}(r) \\ -iU_{\text{aux}}(r) & \end{pmatrix}, \tag{8}$$

where $U_{\text{aux}}(r)$ is a real function

$$U_{\text{aux}}(r) = U_0 \delta_{r,r_0}, \qquad R_{\text{Outer}} \leq r_0 \leq R_{\text{Wall}}. \tag{9}$$

This additional potential does not change the radial Hamiltonian for $r \leq R_{\text{Outer}}$. However, it breaks $\mathscr{T}$ symmetry. The resulting wave function $\psi(r)$ is thus complex in the sense that $\psi(r) \neq \psi^*(r)$.

Determine S matrix from radial wave functions

In asymptotic region,

$$\begin{pmatrix} \psi_{J-1}(r) \\ \psi_{J+1}(r) \end{pmatrix} \longrightarrow \begin{pmatrix} A_{J-1}h^{+}_{J-1}(kr) - B_{J-1}h^{-}_{J-1}(kr) \\ A_{J+1}h^{+}_{J+1}(kr) - B_{J+1}h^{-}_{J+1}(kr) \end{pmatrix},$$

$$\begin{pmatrix} \psi^{*}_{J-1}(r) \\ \psi^{*}_{J+1}(r) \end{pmatrix} \longrightarrow \begin{pmatrix} B^{*}_{J-1}h^{+}_{J-1}(kr) - A^{*}_{J-1}h^{-}_{J-1}(kr) \\ B^{*}_{J+1}h^{+}_{J+1}(kr) - A^{*}_{J+1}h^{-}_{J+1}(kr) \end{pmatrix},$$

the coefficients $A_{J\pm1}$, $B_{J\pm1}$ can be calculated by fitting and satisfy

$$\begin{pmatrix} B_{J-1} \\ B_{J+1} \end{pmatrix} = S \begin{pmatrix} A_{J-1} \\ A_{J+1} \end{pmatrix}, \qquad \begin{pmatrix} A^{*}_{J-1} \\ A^{*}_{J+1} \end{pmatrix} = S \begin{pmatrix} B^{*}_{J-1} \\ B^{*}_{J+1} \end{pmatrix},$$

then S can be unambiguously determined,

$$S = \begin{pmatrix} B_{J-1} & A^{*}_{J-1} \\ B_{J+1} & A^{*}_{J+1} \end{pmatrix} \begin{pmatrix} A_{J-1} & B^{*}_{J-1} \\ A_{J+1} & B^{*}_{J+1} \end{pmatrix}^{-1}.$$

Compare with continuum results

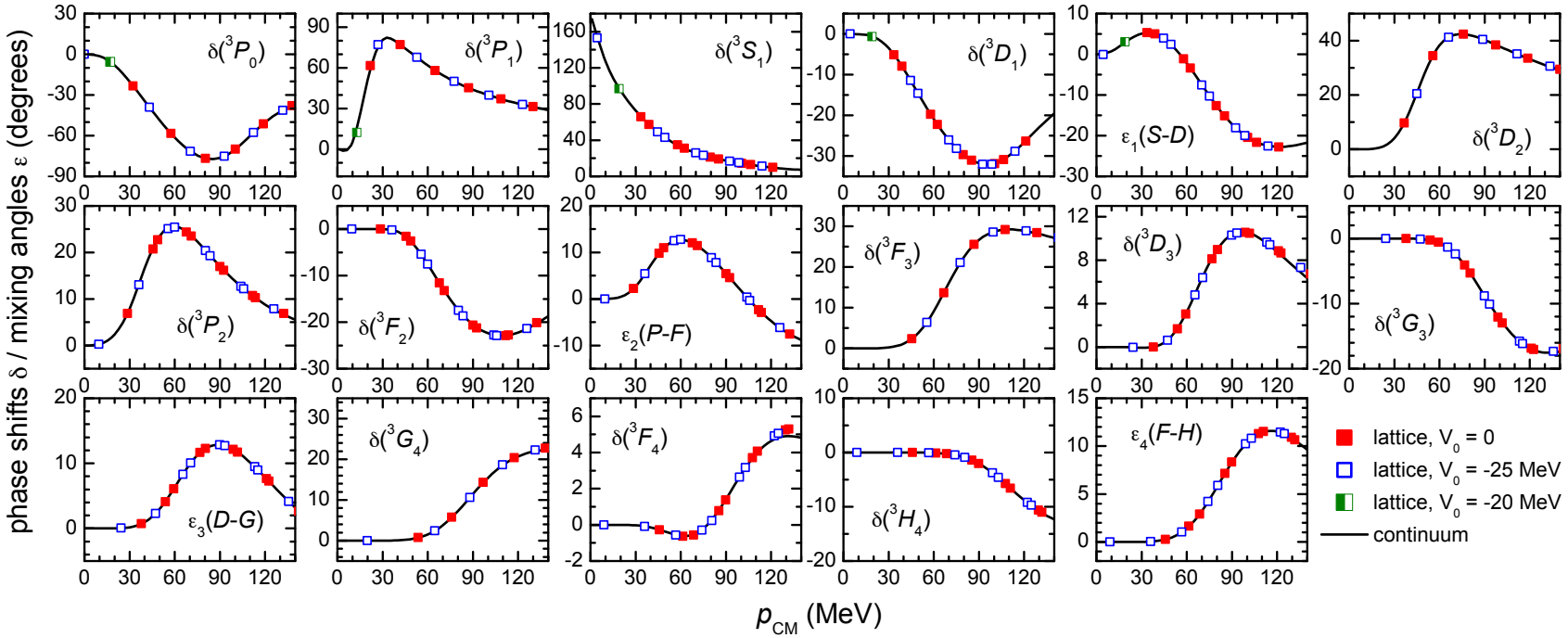

Phase shifts and mixing angles for $J \leq 4$. Both real and complex auxiliary potentials are used. Continuum results are obtained by exactly solving the Lippmann-Schwinger equation.

BNL, Lahde, Lee, Meissner, *Phys. Lett. B* 760, 309 (2016)

Improving the lattice dispersion relation

Lattice dispersion relation

The Laplace operator ∇^2 is discretized as

$$\nabla_L^2 f(\boldsymbol{x}) = \sum_{\boldsymbol{n}} a_{\boldsymbol{n}} f(\boldsymbol{x} + \boldsymbol{n}a).$$

- $N = 2$,
$$-\frac{1}{12a^2} f_{2a}(x) + \frac{4}{3a^2} f_a(x) - \frac{5}{2a^2} f(x),$$
- $N = 3$,
$$\frac{1}{90a^2} f_{3a}(x) - \frac{3}{20a^2} f_{2a}(x) + \frac{3}{2a^2} f_a(x) - \frac{49}{18a^2} f(x),$$

The lattice dispersion relation can be derived as

$$\nabla_L^2 e^{i\boldsymbol{k}\cdot\boldsymbol{r}} = \left(\sum_{\boldsymbol{n}} a_{\boldsymbol{n}} e^{i\boldsymbol{k}\cdot\boldsymbol{n}a} \right) e^{i\boldsymbol{k}\cdot\boldsymbol{r}},$$

where

$$\sum_{\boldsymbol{n}} a_{\boldsymbol{n}} e^{i\boldsymbol{k}\cdot\boldsymbol{n}a} \to -k^2 \quad (a \to 0)$$

Lattice dispersion relation

Approximating the parabola with periodic functions results in lattice artifacts at high momentum.

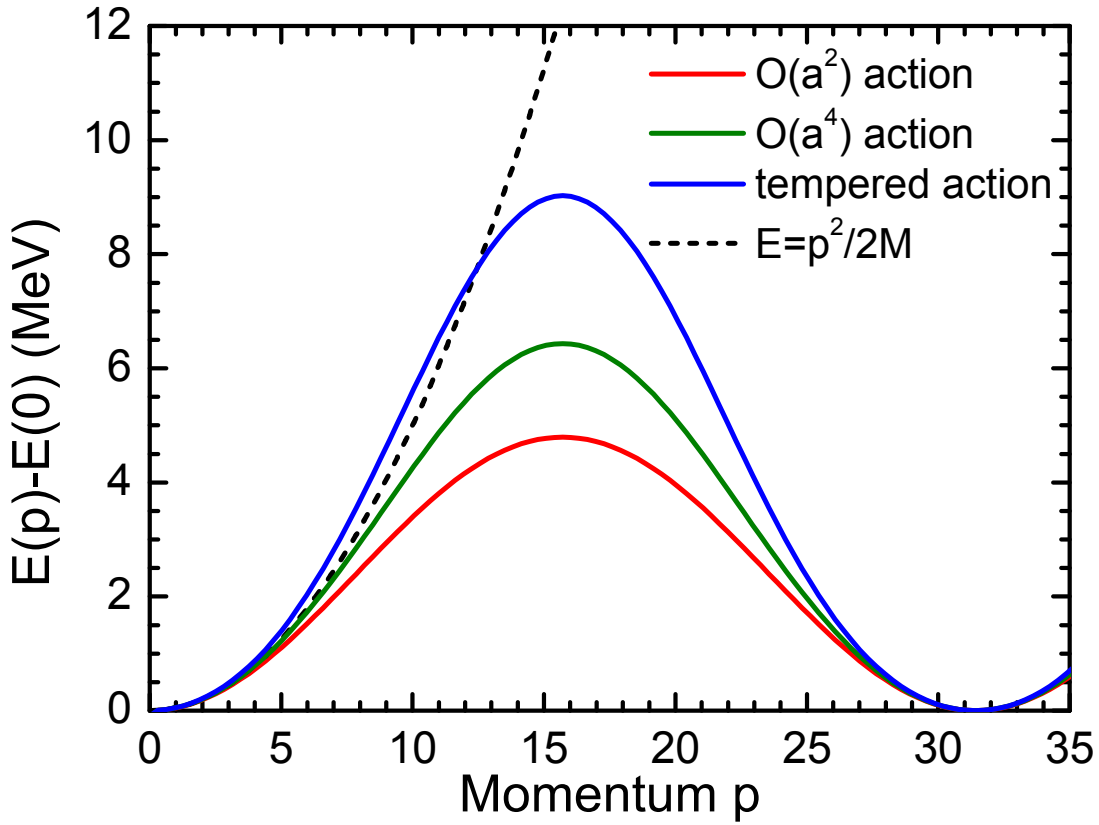

Partial wave lattice dispersion relation

The plane wave expansion

$$e^{i\boldsymbol{k}\cdot\boldsymbol{r}} = 4\pi \sum_{lm} i^l j_l(kr) Y^*_{lm}(\hat{\boldsymbol{k}}) Y_{lm}(\hat{\boldsymbol{r}}),$$

can be inverted,

$$j_l(kr) Y_{lm}(\hat{\boldsymbol{r}}) = \frac{1}{4\pi i^l} \int d\Omega_k e^{i\boldsymbol{k}\cdot\boldsymbol{r}} Y_{lm}(\hat{\boldsymbol{k}}).$$

Applying the lattice dispersion relation for plane waves we get

$$\begin{aligned}
\nabla^2_L j_l(kr) Y_{lm}(\hat{\boldsymbol{r}}) &= \frac{1}{4\pi i^l} \sum_{\boldsymbol{n}} a_{\boldsymbol{n}} \int d\Omega_k e^{i\boldsymbol{k}\cdot\boldsymbol{n}a} e^{i\boldsymbol{k}\cdot\boldsymbol{r}} Y_{lm}(\hat{\boldsymbol{k}}) \\
&= \frac{1}{i^l} \sum_{\boldsymbol{n}} a_{\boldsymbol{n}} \sum_{l'm'} i^{l'} j_{l'}(kr) Y_{l'm'}(\hat{\boldsymbol{r}}) \int d\Omega_k e^{i\boldsymbol{k}\cdot\boldsymbol{n}a} Y^*_{l'm'}(\hat{\boldsymbol{k}}) Y_{lm}(\hat{\boldsymbol{k}}) \\
&\approx \left[\sum_{\boldsymbol{n}} a_{\boldsymbol{n}} \int d\Omega_k e^{i\boldsymbol{k}\cdot\boldsymbol{n}a} |Y_{lm}(\hat{\boldsymbol{k}})|^2 \right] j_l(kr) Y_{lm}(\hat{\boldsymbol{r}}),
\end{aligned}$$

where the angular momentum mixing is ommitted.

Improved partial wave lattice dispersion relation

The partial wave dispersion relations on the lattice reads

$$E(k) = \sum_{\boldsymbol{n}} a_{\boldsymbol{n}} \int d\Omega_k e^{i\boldsymbol{k}\cdot\boldsymbol{n}a} |Y_{lm}(\hat{\boldsymbol{k}})|^2$$

$$= 4\pi \sum_L i^L \left(\sum_n a_n j_L(kna) \right) \left(\sum_{\hat{\boldsymbol{n}}} Y_{L0}(\hat{\boldsymbol{n}}) \right) \left[\sqrt{\frac{2L+1}{4\pi}} C^{l0}_{L0,l0} C^{lm}_{L0,lm} \right],$$

where

$$\tau_L = \sum_{\hat{\boldsymbol{n}}} Y_{L0}(\hat{\boldsymbol{n}}) = \sqrt{\frac{2L+1}{4\pi}} (2P_L(0) + P_L(1)),$$

$$\tau_0 = 3\sqrt{\frac{1}{4\pi}}, \quad \tau_2 = 0, \quad \tau_4 = \frac{21}{4}\sqrt{\frac{1}{4\pi}}, \quad \tau_6 = \frac{3}{8}\sqrt{\frac{13}{4\pi}}, \quad \tau_8 = \frac{99}{64}\sqrt{\frac{17}{4\pi}}$$

For all (l, m) combination $E(k) \to -k^2$ in the continuum limit.

Improved partial wave lattice dispersion relation

For $J \leq 4$ we have

$$E_{1\,S_0 A_1}(p) = E_{1\,P_1 T_1}(p) = \sum_n a_n \left[3 j_0(pna)\right],$$

$$E_{1\,D_2 E}(p) = \sum_n a_n \left[3 j_0(pna) + \frac{9}{2} j_4(pna)\right],$$

$$E_{1\,F_3 T_1}(p) = \sum_n a_n \left[3 j_0(pna) + \frac{63}{22} j_4(pna) - \frac{25}{22} j_6(pna)\right],$$

with j_0, j_2 and j_4 the spherical Bessel functions.

Suppression of the free-space phase shift

The lattice artifacts in the dispersion relation and the unphysical phase shifts can be suppressed by introducing higher-order corrections.

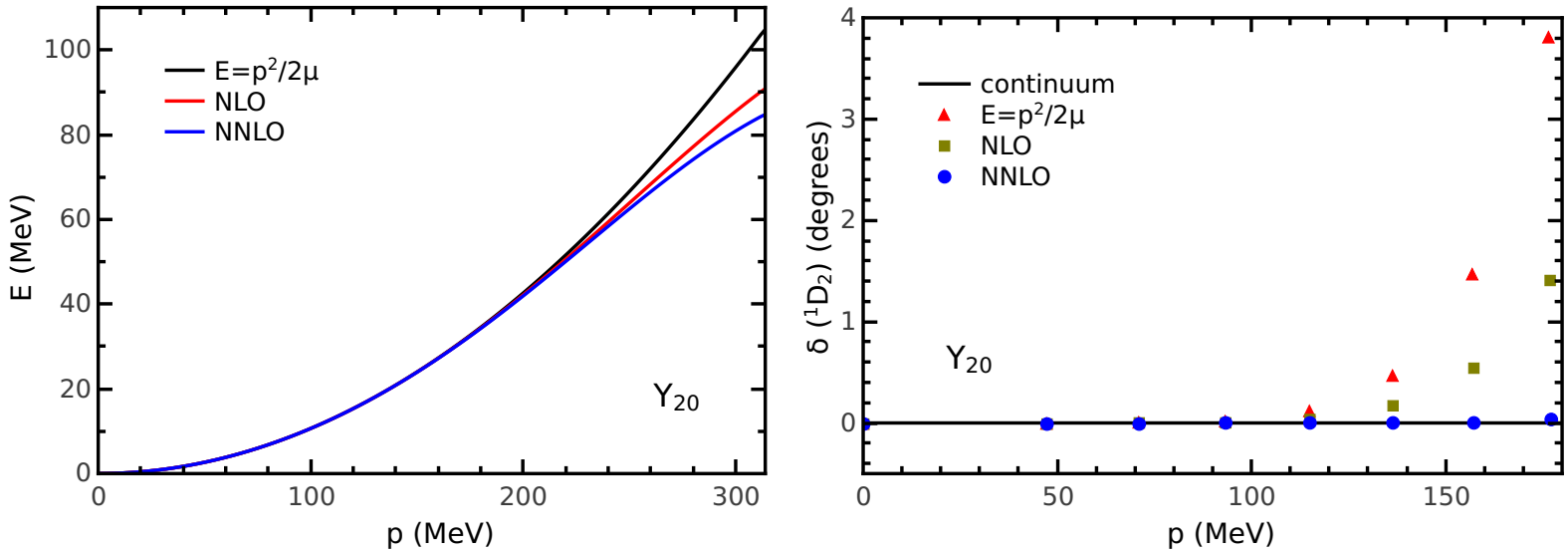

Left panel: Dispersion relations in the continuum $E = p^2/2\mu$ (black curve), with leading order correction (red curve) and with next-to-leading order correction (blue curve).

Right panel: Phase shifts for ${}^1D_2(E)$ partial wave calculated without potential and with various dispersion relations.

Phase shifts with improved dispersion relations

The accuracy can be preserved to higher momentum using the improved dispersion relations.

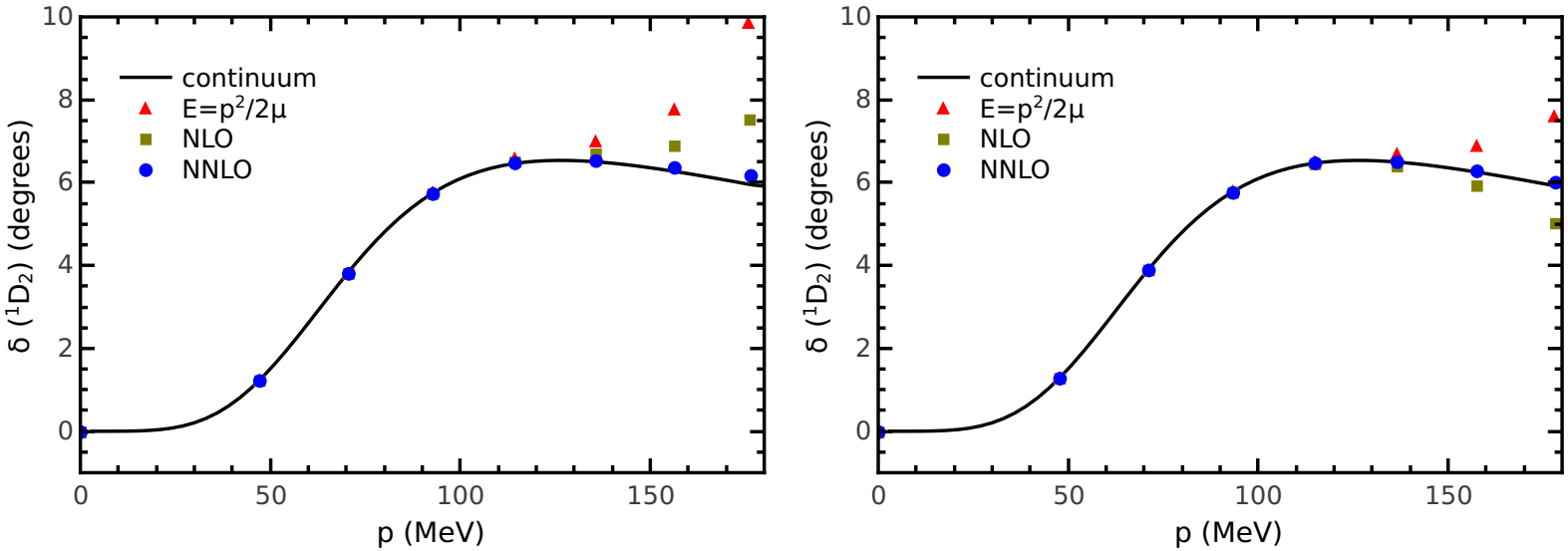

Left panel: Phase shifts for ${}^1D_2(E)$ partial wave calculated with various dispersion relations.

Right panel: Same, for ${}^1D_2(T)$ partial wave.

Analysis of phase shift in the NLEFT

Realistic chiral NN force

We define the transfer matrix as

$$M \equiv : \exp(-a_t H) :,$$

with the Hamiltonian

$$H = H_{\text{free}} + V_{\text{LO}} + V_{\text{NLO}} + \ldots,$$

where $H_{\text{free}}$is the free nucleon Hamiltonian,

$$\begin{aligned} H_{\text{free}} \quad = \quad & \frac{3\omega_0}{m_N} \sum_{\boldsymbol{n}} \sum_{i,j=0,1} a^\dagger_{i,j}(\boldsymbol{n}) a_{i,j}(\boldsymbol{n}) \\ & - \frac{\omega_1}{2m_N} \sum_{\boldsymbol{n}} \sum_{l=1}^{3} \sum_{i,j=0,1} \left[a^\dagger_{i,j}(\boldsymbol{n}) a_{i,j}(\boldsymbol{n}+\hat{\boldsymbol{e}}_l) + a^\dagger_{i,j}(\boldsymbol{n}) a_{i,j}(\boldsymbol{n}-\hat{\boldsymbol{e}}_l) \right] \\ & + \frac{\omega_2}{2m_N} \sum_{\boldsymbol{n}} \sum_{l=1}^{3} \sum_{i,j=0,1} \left[a^\dagger_{i,j}(\boldsymbol{n}) a_{i,j}(\boldsymbol{n}+2\hat{\boldsymbol{e}}_l) + a^\dagger_{i,j}(\boldsymbol{n}) a_{i,j}(\boldsymbol{n}-2\hat{\boldsymbol{e}}_l) \right] \\ & - \frac{\omega_3}{2m_N} \sum_{\boldsymbol{n}} \sum_{l=1}^{3} \sum_{i,j=0,1} \left[a^\dagger_{i,j}(\boldsymbol{n}) a_{i,j}(\boldsymbol{n}+3\hat{\boldsymbol{e}}_l) + a^\dagger_{i,j}(\boldsymbol{n}) a_{i,j}(\boldsymbol{n}-3\hat{\boldsymbol{e}}_l) \right] \end{aligned}$$

Interaction expansion up to NNLO

The potential terms are given by

$$
\begin{aligned}
V_{\mathrm{LO}} =& C_{^1S_0}\mathscr{O}^{(0)}_{(0,1)} + C_{^3S_1}\mathscr{O}^{(0)}_{(1,0)} + V^{(0)}_{\mathrm{OPE}},\\
V_{\mathrm{NLO}} =& C_{q^2}\mathscr{O}^{(2)}_{1} + C_{I^2,q^2}\mathscr{O}^{(2)}_{2} + C_{S^2,q^2}\mathscr{O}^{(2)}_{3}\\
&+ C_{S^2,I^2,q^2}\mathscr{O}^{(2)}_{4} + C_{(\boldsymbol{q}\cdot\boldsymbol{S})^2}\mathscr{O}^{(2)}_{5}\\
&+ C_{I^2,(\boldsymbol{q}\cdot\boldsymbol{S})^2}\mathscr{O}^{(2)}_{6} + C^{I=1}_{(\boldsymbol{q}\times\boldsymbol{S})\cdot\boldsymbol{k}}\mathscr{O}^{(2)}_{7}\\
&+ V^{(2)}_{\mathrm{TPE}} + V^{(2)}_{\mathrm{IB}} + V_{\mathrm{Coulomb}}\\
V_{\mathrm{NNLO}} =& V^{(3)}_{\mathrm{TPE}}.
\end{aligned}
$$

At LO we use the pion mass M_{π^0} for all channels. The resulting Isospin Breaking (IB) effects are included at NLO. The Coulomb force is also included at NLO. We neglect these terms for neutron-proton scattering.

Contact terms at leading order

The LO interaction contains two contact terms and the LO 1-pion exchange potential.
The two LO contact terms

$$\mathscr{O}_1^{(0)} = \frac{1}{2} : \sum_{\boldsymbol{n}} \rho(\boldsymbol{n})\rho(\boldsymbol{n}) :, \qquad \mathscr{O}_2^{(0)} = \frac{1}{2} \sum_{\boldsymbol{n}} \sum_{I} : \rho_I(\boldsymbol{n})\rho_I(\boldsymbol{n}) :$$

are adjusted to the ${}^1S_0$ and ${}^3S_1$ partial wave phase shifts. A better description of the S waves are given by the smeared contact terms,

$$\mathscr{O}_1^{(0)} \to \frac{1}{2L^3} : \sum_{\boldsymbol{q}} f(\boldsymbol{q})\rho(\boldsymbol{q})\rho(-\boldsymbol{q}) :, \quad \mathscr{O}_2^{(0)} \to \frac{1}{2L^3} : \sum_{\boldsymbol{q}} f(\boldsymbol{q})\rho_I(\boldsymbol{q})\rho_I(-\boldsymbol{q}) :,$$

where $f(\boldsymbol{q})$ is a smooth cutoff function in momentum space,

$$f(\boldsymbol{q}) = (\text{Normalization} \quad \text{Constant}) \times \exp\left(-b_s \frac{q^4}{4}\right)$$

Contact terms at leading order

A by-product of the operator smearing is the unwanted attracted fores in higher partial waves.
For P waves only the pion-exchange interactions should contribute.
We introduce the projection operators

$$P^{(0,1)} = \left(\frac{1}{4} - \frac{\boldsymbol{\sigma}_1 \cdot \boldsymbol{\sigma}_2}{4}\right)\left(\frac{3}{4} + \frac{\vec{\tau}_1 \cdot \vec{\tau}_2}{4}\right),$$
$$P^{(1,0)} = \left(\frac{3}{4} + \frac{\boldsymbol{\sigma}_1 \cdot \boldsymbol{\sigma}_2}{4}\right)\left(\frac{1}{4} - \frac{\vec{\tau}_1 \cdot \vec{\tau}_2}{4}\right)$$

to the $(S, I) = (0, 1)$ or $(1, 0)$ channels. The force in P-wave is eliminated by the constraint of wave function antisymmetrization.

Contact terms at LO

The final version of LO contact terms is

$$\begin{aligned}
\mathscr{O}^{(0)}_{(0,1)} &= \frac{3}{32L^3}:\sum_{\boldsymbol{q}} f(\boldsymbol{q})\rho(\boldsymbol{q})\rho(-\boldsymbol{q}):-\frac{3}{32L^3}:\sum_{\boldsymbol{q}} f(\boldsymbol{q})\sum_{S}\rho_S(\boldsymbol{q})\rho_S(-\boldsymbol{q}):\\
&\quad+\frac{1}{32L^3}:\sum_{\boldsymbol{q}} f(\boldsymbol{q})\sum_{I}\rho_I(\boldsymbol{q})\rho_I(-\boldsymbol{q}):-\frac{1}{32L^3}:\sum_{\boldsymbol{q}} f(\boldsymbol{q})\sum_{S,I}\rho_{S,I}(\boldsymbol{q})\rho_{S,I}(-\boldsymbol{q}):,\\
\mathscr{O}^{(0)}_{(1,0)} &= \frac{3}{32L^3}:\sum_{\boldsymbol{q}} f(\boldsymbol{q})\rho(\boldsymbol{q})\rho(-\boldsymbol{q}):+\frac{1}{32L^3}:\sum_{\boldsymbol{q}} f(\boldsymbol{q})\sum_{S}\rho_S(\boldsymbol{q})\rho_S(-\boldsymbol{q}):\\
&\quad-\frac{3}{32L^3}:\sum_{\boldsymbol{q}} f(\boldsymbol{q})\sum_{I}\rho_I(\boldsymbol{q})\rho_I(-\boldsymbol{q}):-\frac{1}{32L^3}:\sum_{\boldsymbol{q}} f(\boldsymbol{q})\sum_{S,I}\rho_{S,I}(\boldsymbol{q})\rho_{S,I}(-\boldsymbol{q}):
\end{aligned}$$

with the density operators defined as

$$\rho(\boldsymbol{n})=\sum_{i,j} a^\dagger_{i,j}(\boldsymbol{n})a_{i,j}(\boldsymbol{n}),\qquad \rho_I(\boldsymbol{n})=\sum_{i,j,j'} a^\dagger_{i,j}(\boldsymbol{n})(\tau_I)_{j,j'}a_{i,j'}(\boldsymbol{n})$$

$$\rho_S(\boldsymbol{n})=\sum_{i,i',j} a^\dagger_{i,j'}(\boldsymbol{n})(\sigma_S)_{i,i'}a_{i',j}(\boldsymbol{n}),\qquad \rho_{S,I}(\boldsymbol{n})=\sum_{i,i',j,j'} a^\dagger_{i,j}(\boldsymbol{n})(\sigma_S)_{i,i'}(\tau_I)_{j,j'}a_{i',j'}(\boldsymbol{n}),$$

Long-range pion-exchange potential at LO

At LO the One-Pion-Exchange potential (OPEP) is given by

$$V_{\mathrm{OPE}}^{(0)}(M_\pi) = -\frac{g_A^2}{8F_\pi^2} \sum_{S_1,S_2,I} \sum_{\boldsymbol{n_1},\boldsymbol{n_2}} G_{S_1,S_2}(\boldsymbol{n}_1 - \boldsymbol{n}_2, M_\pi) \rho_{S_1,I}(\boldsymbol{n}_1) \rho_{S_2,I}(\boldsymbol{n}_2),$$

with the pion propagator

$$G_{S_1,S_2}(\boldsymbol{n}_1 - \boldsymbol{n}_2, M_\pi) = \frac{1}{L^3} \sum_{\boldsymbol{k}} \exp\left[i \frac{2\pi}{L} \boldsymbol{k} \cdot (\boldsymbol{n}_1 - \boldsymbol{n}_2) \right] G_{S_1,S_2}(\boldsymbol{k}, M_\pi),$$

where

$$G_{S_1,S_2}(\boldsymbol{k}, M_\pi) = \frac{q_{S_1} q_{S_2}}{q^2 + M_\pi^2}, \qquad \boldsymbol{q} = \frac{2\pi}{L} \boldsymbol{k}.$$

$g_A = 1.29$, $F_\pi = 92.2$ MeV, $M_\pi = 139.57$ MeV for $\pi^\pm$ and 134.98 MeV for π^0. Fast Fourier Transform are used to calculate the lattice OPEP at LO.

Contact terms at NLO

The seven NLO contact terms with two derivatives are

$$\mathscr{O}_1^{(2)} = -\frac{1}{2} :\sum_{\boldsymbol{n}}\sum_{I}\rho(\boldsymbol{n})\nabla_I^2\rho(\boldsymbol{n}):, \mathscr{O}_2^{(2)} = -\frac{1}{2} :\sum_{\boldsymbol{n}}\sum_{I,I}\rho_I(\boldsymbol{n})\nabla_I^2\rho_I(\boldsymbol{n}):,$$

$$\mathscr{O}_3^{(2)} = -\frac{1}{2} :\sum_{\boldsymbol{n}}\sum_{S,I}\rho_S(\boldsymbol{n})\nabla_I^2\rho_S(\boldsymbol{n}):, \mathscr{O}_4^{(2)} = -\frac{1}{2}\sum_{\boldsymbol{n}}\sum_{S,I}\rho_{S,I}(\boldsymbol{n})\nabla_I^2\rho_{S,I}(\boldsymbol{n}):,$$

$$\mathscr{O}_5^{(2)} = \frac{1}{2} :\sum_{\boldsymbol{n}}\sum_{S}\nabla_S\rho_S(\boldsymbol{n})\sum_{S'}\nabla_{S'}\rho_{S'}(\boldsymbol{n}) :\mathscr{O}_6^{(2)} == \frac{1}{2} :\sum_{\boldsymbol{n}}\sum_{S}\nabla_S\rho_{S,I}(\boldsymbol{n})\sum_{S'}\nabla_{S'}\rho_{S'}(\boldsymbol{n}) :$$

$$\mathscr{O}_7^{(2)} = -\frac{i}{2}\left[\frac{3}{4} :\sum_{\boldsymbol{n}}\sum_{I,S,I'}\varepsilon_{I,S,I'}\left(\Pi_I(\boldsymbol{n})\nabla_{I'}\rho_S(\boldsymbol{n}) + \Pi_{I,S}(\boldsymbol{n})\nabla_{I'}\rho(\boldsymbol{n})\right):\right]$$

$$-\frac{i}{2}\left[\frac{1}{4} :\sum_{\boldsymbol{n}}\sum_{I,S,I',I}\varepsilon_{I,S,I'}\left(\Pi_{I,I}(\boldsymbol{n})\nabla_{I'}\rho_{S,I}(\boldsymbol{n}) + \Pi_{I,S,I}(\boldsymbol{n})\nabla_{I'}\rho_I(\boldsymbol{n})\right):\right],$$

where the finite difference formula is used for numerical derivatives,

$$\nabla_I f(\boldsymbol{n}) = \frac{1}{2a}\left[f(\boldsymbol{n}+a\hat{\boldsymbol{e}}_I) - f(\boldsymbol{n}-a\hat{\boldsymbol{e}}_I)\right].$$

Pion-exchange potential at NLO

At NLO the Two-Pion Exchange Potential (TPEP) is included explicitly,

$$V_{\rm TPE}^{(2)} = \sum_{\boldsymbol{n_1}\boldsymbol{n_2}}\sum_{S_1 S_2} T^{(2)}_{S_1,S_2}(\boldsymbol{n}_1-\boldsymbol{n}_2)\rho_{S_1}(\boldsymbol{n}_1)\rho_{S_2}(\boldsymbol{n}_2) + \sum_{\boldsymbol{n_1}\boldsymbol{n_2}}\sum_{I} W_C^{(2)}(\boldsymbol{n}_1-\boldsymbol{n}_2)\rho_I(\boldsymbol{n}_1)\rho_I(\boldsymbol{n}_2)$$
$$+ \sum_{\boldsymbol{n_1}\boldsymbol{n_2}}\sum_{S} V_S^{(2)}(\boldsymbol{n}_1-\boldsymbol{n}_2)\rho_S(\boldsymbol{n}_1)\rho_S(\boldsymbol{n}_2),$$

where the functions T, W_C and V_S are Fourier transforms of

$$\begin{aligned} T^{(2)}_{S_1,S_2}(\boldsymbol{k}) &= 18 g_A^4 F^{(2)}(\boldsymbol{q}) q_{S_1} q_{S_2}, \\ W_C^{(2)}(\boldsymbol{k}) &= F^{(2)}(\boldsymbol{q})\left[\frac{48 g_A^2 M_\pi^4}{q^2+4M_\pi^2} + 4M_\pi^2(5g_A^4-4g_A^2-1) + q^2(23g_A^4-10g_A^2-1)\right] \\ V_S^{(2)}(\boldsymbol{k}) &= -18 g_A^4 F^{(2)}(\boldsymbol{q}) q^2, \end{aligned}$$

with

$$F^{(2)}(\boldsymbol{q}) = -\frac{1}{768\pi^2 F_\pi^4}\frac{\sqrt{4M_\pi^2+q^2}}{2|\boldsymbol{q}|}\ln\left(\frac{\sqrt{q^2+4M_\pi^2}+|\boldsymbol{q}|}{\sqrt{q^2+4M_\pi^2}-|\boldsymbol{q}|}\right)$$

Pion-exchange potential and NNLO

At NNLO the TPEP reads,

$$V_{\rm TPE}^{(3)} = \sum_{\boldsymbol{n_1}\boldsymbol{n_2}}\sum_{S_1 S_2 I} T^{(3)}_{S_1,S_2}(\boldsymbol{n}_1-\boldsymbol{n}_2)\rho_{S_1,I}(\boldsymbol{n}_1)\rho_{S_2,I}(\boldsymbol{n}_2) + \sum_{\boldsymbol{n_1}\boldsymbol{n_2}}\sum_{S,I} W_S^{(3)}(\boldsymbol{n}_1-\boldsymbol{n}_2)\rho_{S,I}(\boldsymbol{n}_1)\rho_{S,I}(\boldsymbol{n}_2) + \sum_{\boldsymbol{n_1}\boldsymbol{n_2}} V_C^{(3)}(\boldsymbol{n}_1-\boldsymbol{n}_2)\rho(\boldsymbol{n}_1)\rho(\boldsymbol{n}_2),$$

where the functions T, W_S and V_C are Fourier transforms of

$$\begin{aligned} T^{(3)}_{S_1,S_2}(\boldsymbol{k}) &= c_4 F^{(3)}(\boldsymbol{q})(q^2+4M_\pi^2) q_{S_1} q_{S_2}, \\ W_S^{(3)}(\boldsymbol{k}) &= -c_4 F^{(3)}(\boldsymbol{q}) q^2 \\ V_C^{(3)}(\boldsymbol{k}) &= 6F^{(3)}(\boldsymbol{q})(q^2+2M_\pi^2)\left[2M_\pi^2(2c_1-c_3)-c_3 q^2\right], \end{aligned}$$

with

$$F^{(3)}(\boldsymbol{q}) = -\frac{g_A^2}{64\pi f_\pi^4}\times\frac{1}{2|\boldsymbol{q}|}\arctan\left(\frac{|\boldsymbol{q}|}{2M_\pi}\right).$$

S-wave phase shift at LO

The smeared contact interactions are fitted to Nigmegen Partial Wave Analysis (NPWA).

"Partial-wave analysis of all nucleon-nucleon scattering data below 350 MeV"
V. G. J. Stoks, et. al., Phys. Rev. C 48 (1993) 792

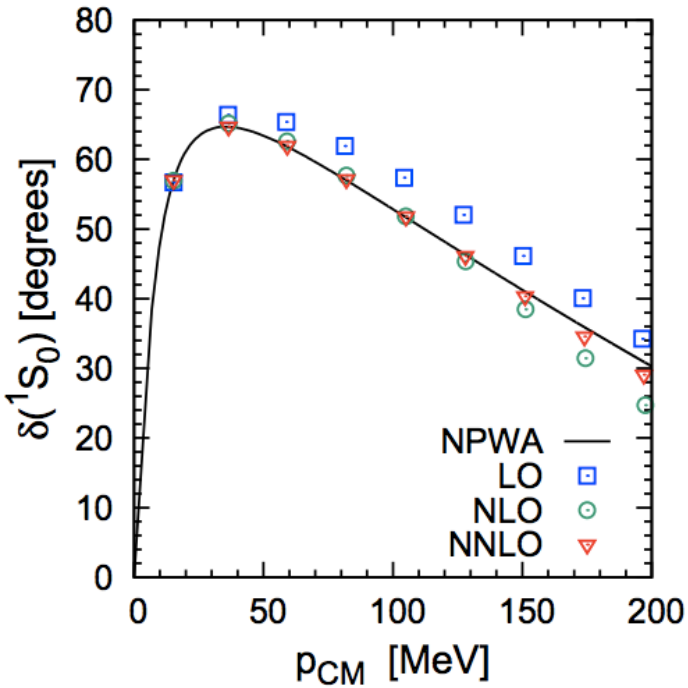

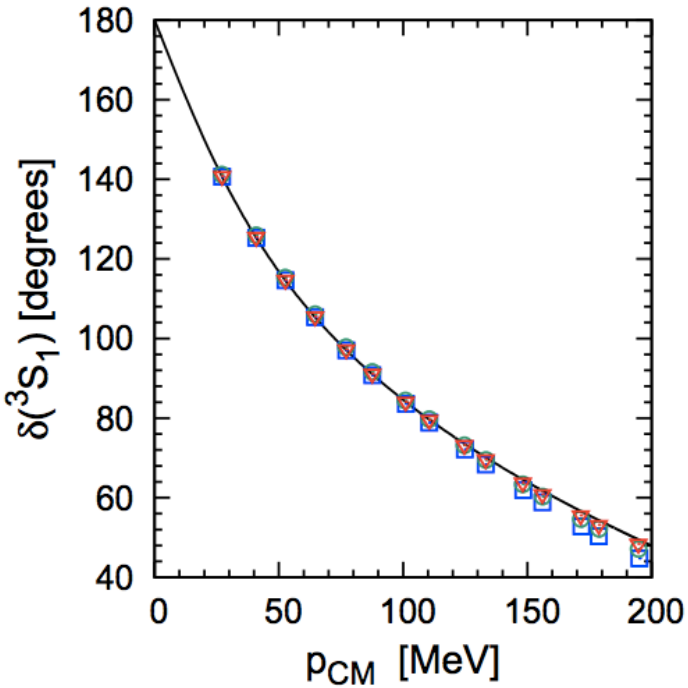

LECs' up to NNLO

order	fit parameters	$a = 1.97$ fm	$a = 1.64$ fm	$a = 1.32$ fm
LO	$C_{^1S_0}$	$-0.4676(2)$	$-0.3290(7)$	$-0.201(5)$
	$C_{^3S_1}$	$-0.6377(2)$	$-0.4482(2)$	$-0.265(5)$
	b_s	$0.0524(2)$	$0.0917(2)$	$0.173(6)$
NLO	$C_{^1S_0}$	$-0.5(1)$	$-0.35(2)$	$-0.220(2)$
	$C_{^3S_1}$	$-0.44(7)$	$-0.21(1)$	$-0.152(4)$
	C_{q^2}	$-0.05(3)$	$-0.032(9)$	$-0.006(1)$
	C_{I^2,q^2}	$0.08(2)$	$0.075(2)$	$0.052(1)$
	C_{S^2,q^2}	$-0.06(3)$	$-0.046(3)$	$-0.0341(7)$
	C_{S^2,I^2,q^2}	$0.03(2)$	$0.029(2)$	$0.0081(2)$
	$C_{(q\cdot S)^2}$	$0.11(2)$	$0.091(4)$	$0.0553(2)$
	$C_{I^2,(q\cdot S)^2}$	$-0.11(2)$	$-0.074(4)$	$-0.0240(8)$
	$C^{I=1}_{(q\times S)\cdot k}$	$0.037(8)$	$0.026(4)$	$0.019(2)$
NNLO	$C_{^1S_0}$	$-0.5(1)$	$-0.33(4)$	$-0.21(2)$
	$C_{^3S_1}$	$-0.5(1)$	$-0.22(1)$	$-0.15(2)$
	C_{q^2}	$0.08(3)$	$0.093(7)$	$0.118(7)$
	C_{I^2,q^2}	$0.07(2)$	$0.0668(4)$	$0.045(4)$
	C_{S^2,q^2}	$-0.06(3)$	$-0.05(2)$	$-0.036(7)$
	C_{S^2,I^2,q^2}	$0.01(2)$	$0.005(3)$	$-0.014(4)$
	$C_{(q\cdot S)^2}$	$0.10(3)$	$0.086(7)$	$0.056(4)$
	$C_{I^2,(q\cdot S)^2}$	$-0.10(3)$	$-0.055(4)$	$-0.006(4)$
	$C^{I=1}_{(q\times S)\cdot k}$	$0.031(8)$	$0.025(4)$	$0.018(2)$

S-wave scattering parameters from NLEFT

Low-energy S-wave parameters. E_d is the deuteron binding energy, and the a_i and r_i denote the scattering lengths and effective ranges in channel i, respectively.
The deuteron binding energy is not used in the LO fit.

order	a [fm]	E_d [MeV]	$r_{^1S_0}$ [fm]	$a_{^1S_0}$ [fm]	$r_{^3S_1}$ [fm]	$a_{^3S_1}$ [fm]
LO	1.97	2.00(1)	2.041(1)	−22.4(4)	1.686(1)	5.46(1)
	1.64	2.07(1)	2.093(5)	−22.5(7)	1.6932(8)	5.45(1)
	1.32	2.12(2)	2.11(2)	−22.5(5)	1.71(1)	5.44(1)
NLO	1.97	2.2246(3)†	2.4(6)	−23(4)	1.79(3)	5.31(2)
	1.64	2.2246(1)†	2.3(1)	−23(2)	1.73(1)	5.33(1)
	1.32	2.2246(1)†	2.47(3)	−23(1)	1.70(1)	5.336(9)
NNLO	1.97	2.2246(3)†	2.6(6)	−24(4)	1.82(3)	5.35(2)
	1.64	2.2246(1)†	2.5(3)	−23(2)	1.74(1)	5.36(1)
	1.32	2.22457(7)†	2.6(2)	−23(1)	1.744(7)	5.382(5)
experiment	–	2.224575(9)	2.77(5)	−23.740(20)	1.753(8)	5.419(7)

Phase shifts from NLEFT (a^{-1}=200 MeV)

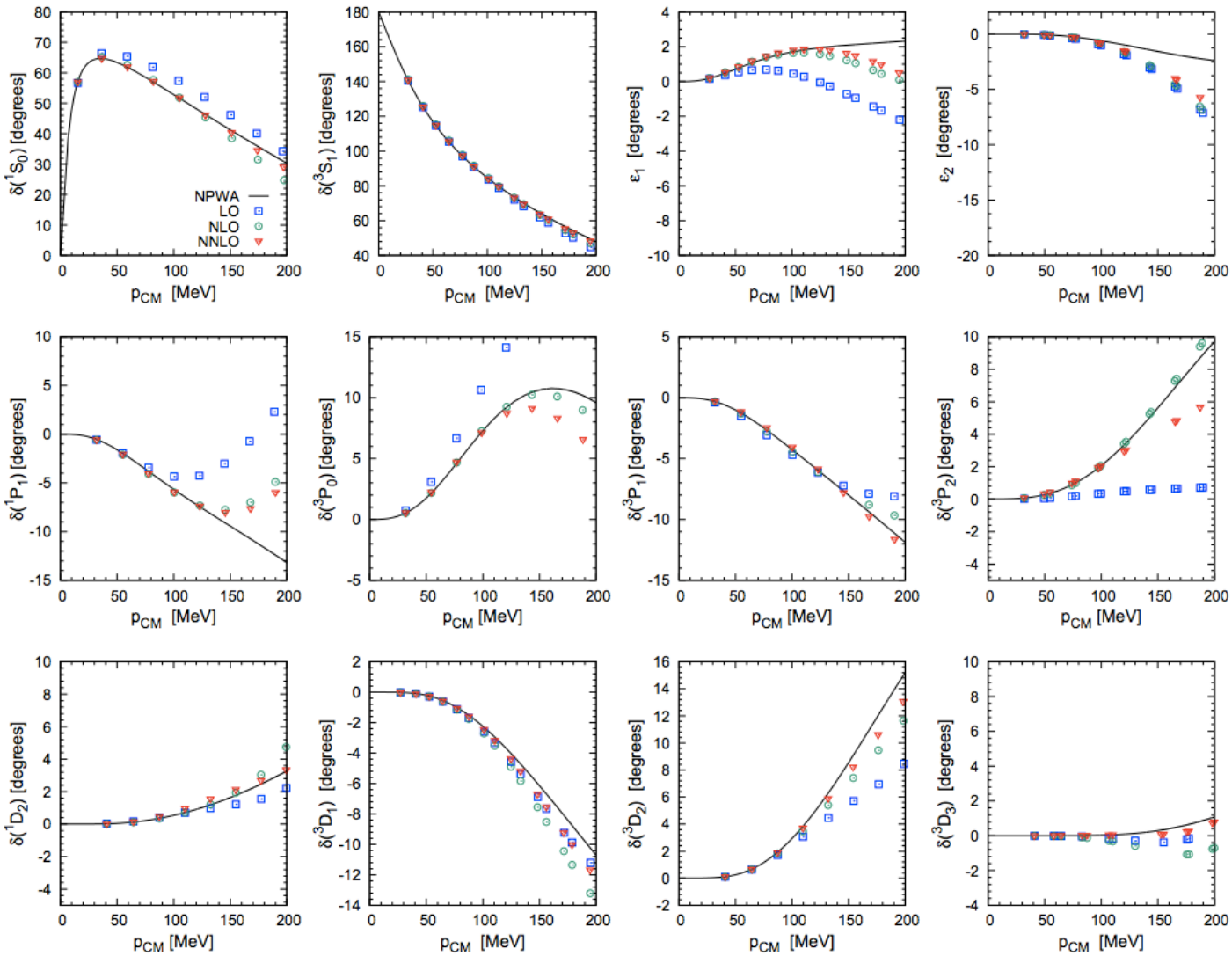

Phase shifts from NLEFT (a^{-1}=150 MeV)

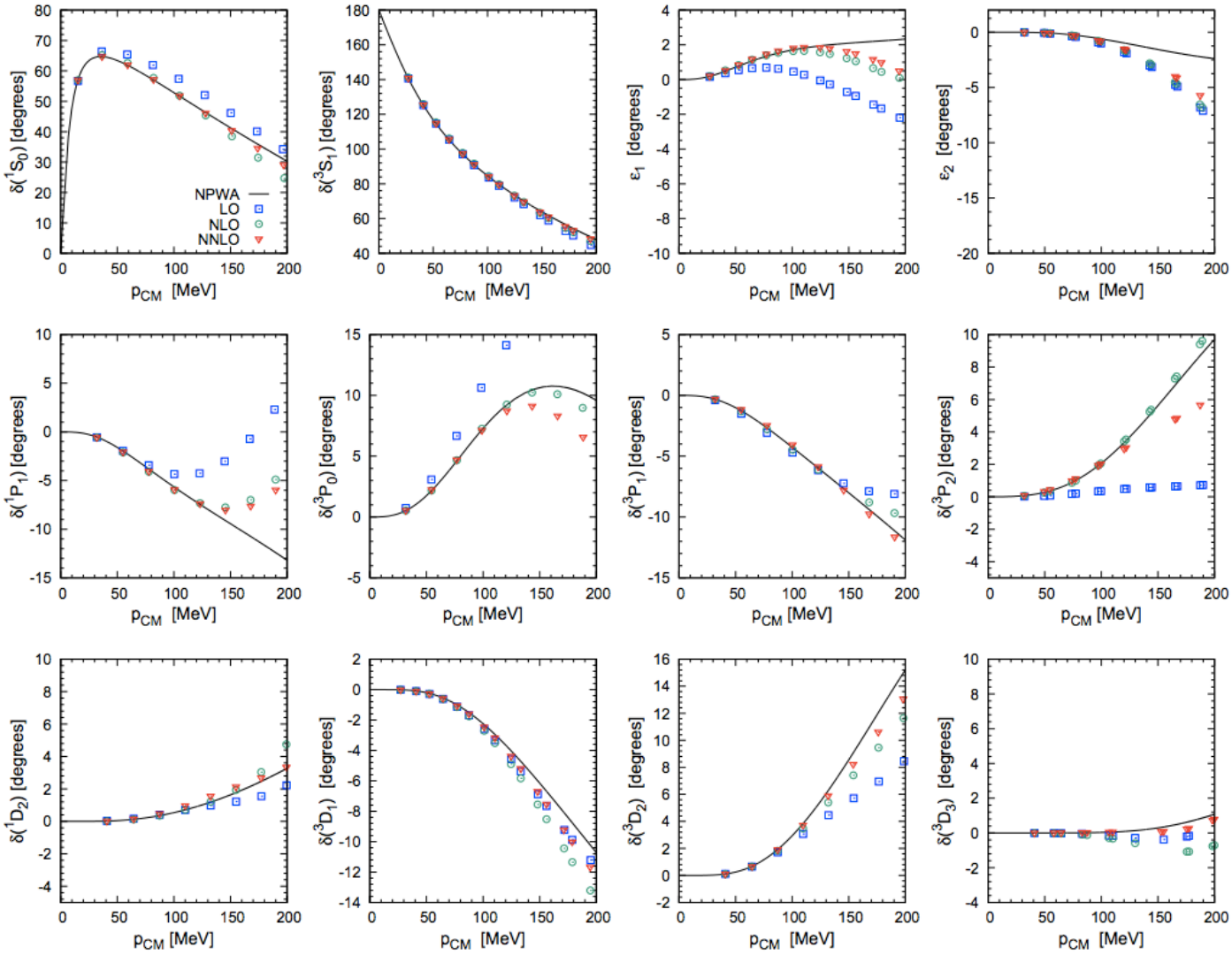

Phase shifts from NLEFT (a^{-1}=100 MeV)

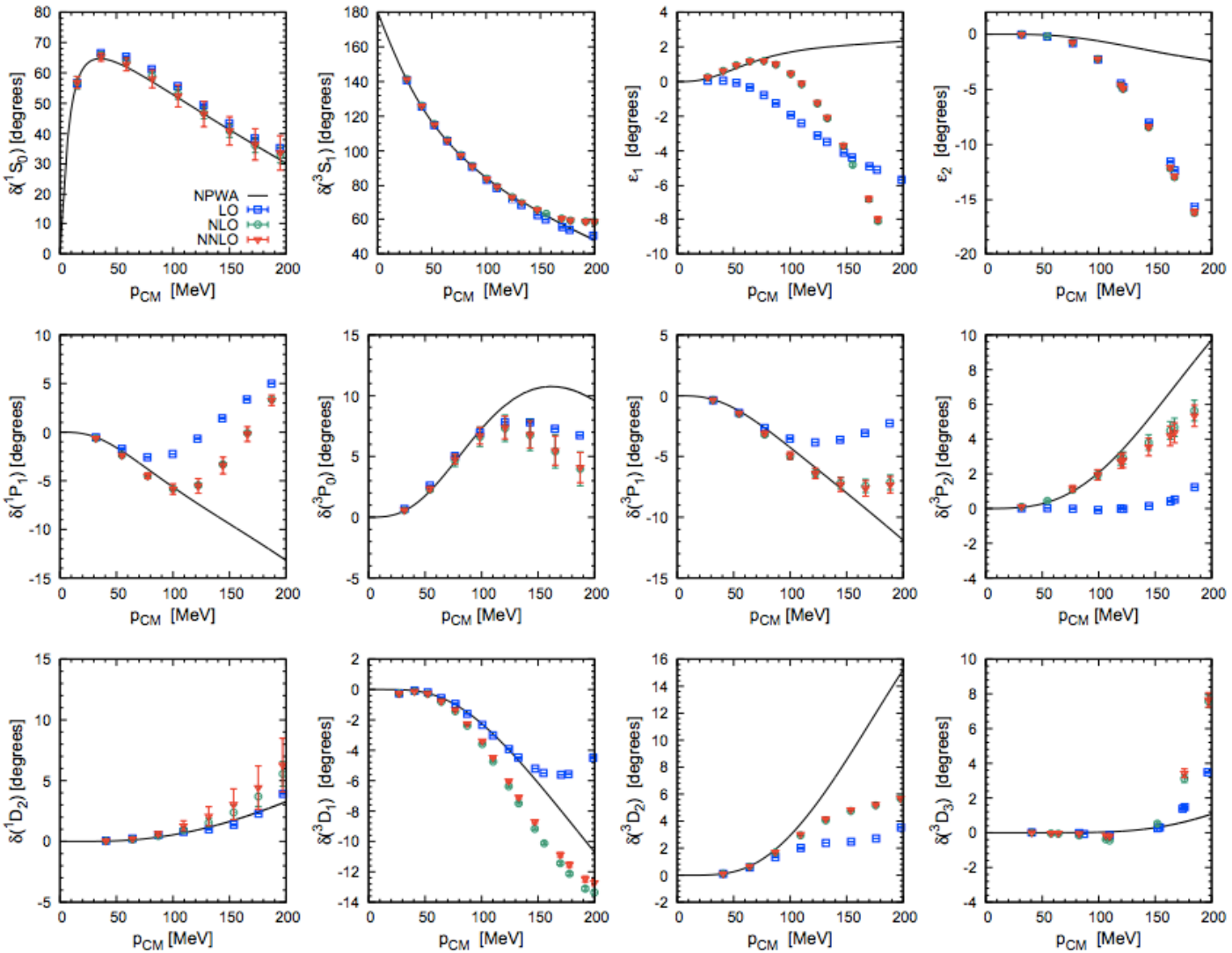

Nuclear Binding energies from NLEFT (up to NNLO)

The nuclear binding energies with 2N forces up to NNLO in the NLEFT for $a^{-1} = 100$ MeV. All energies are in MeV. The uncertainties in the parathnesses are from Monte Carlo simulation.

	$E_B^{NNLO}(2N)$	$E_B(exp)$
^{4}He	-25.60(6)	-28.30
^{8}Be	-48.6(1)	-56.35
^{12}C	-78.7(2)	-92.16
^{16}O	-121.4(5)	-127.62
^{20}Ne	-163.6(9)	-160.64
^{24}Mg	-208(2)	-198.26
^{28}Si	-275(3)	-236.54

Summary

- The lattice results are distorted by artifacts. The rotational symmetry as well as the energy-momentum dispersion relation need to be corrected for the precision calculation of the phase shifts.
- The lattice artifacts vanish for $a \to 0$ and $L \to \infty$. For practical calculations these conditions are usually not met. For finite lattice spacings and finite volumes we developed several algorithms and approximating formulae to get rid of the artifacts. The resulting phase shifts are accurate enough to fit to the data.
- We fit the NLEFT low energy constants up to third order (NNLO) to the Nijmegen PWA. The resulting phase shifts and mixing angles are improved for either using finer lattice or including higher order terms in the calculation. We expect a $\mathrm{N^3LO}$ analysis on the lattice would confirm these findings.